New estimate of organic carbon export from optical measurements reveals the role of particle size distribution and export depth

D.J. Clements[1], S. Yang[1], T. Weber[2], A.M.P. McDonnell[3], R.Kiko[45], L.Stemmann[4], D.Bianchi[1]

[1]Department of Atmospheric and Oceanic Sciences, University of California Los Angeles, Los Angeles, CA, USA.
[2]Department of Earth and Environmental Sciences, University of Rochester,Rochester, New York, USA
[3]College of Fisheries and Ocean Sciences, University of Alaska Fairbanks, Fairbanks, Alaska 99775-7220, USA.
[4]Sorbonne Université, CNRS, UMR 7093, Institut de la Mer de Villefranche sur mer, Laboratoire d'Océanographie de Villefranche, Villefranche-sur-Mer, France.
[5]Biological Oceanography, Helmholtz Center for Ocean Research Kiel, Kiel, Germany.

Key Points:

- We present a new estimate of sinking particulate carbon fluxes from the surface ocean from global reconstructions of particle size distribution.
- Smaller particles contribute more to the total sinking carbon flux than large particles.
- Carbon flux estimates from multiple depth horizons suggest net heterotrophy in the deeper euphotic zone, rather than autotrophy.

Corresponding author: D.J Clements, dclements@atmos.ucla.edu

Abstract

Export of sinking particles from the surface ocean is critical for carbon sequestration and to provide energy to the deep biosphere. The magnitude and spatial patterns of this export have been estimated in the past by *in situ* particle flux observations, satellite-based algorithms, and ocean biogeochemical models; however, these estimates remain uncertain. Here, we use a recent machine learning reconstruction of global ocean particle size distributions from Underwater Vision Profiler 5 (UVP5) measurements to estimate carbon fluxes by sinking particles (35 μm - 5 mm equivalent spherical diameter) from the surface ocean. We combine global maps of particle size distribution properties with empirical relationships constrained against *in situ* flux observations to calculate particulate carbon export from the euphotic zone and wintertime mixed layer depths. The new flux reconstructions suggest a less variable seasonal cycle in the tropical ocean, and a more persistent export in the Southern Ocean than previously recognized. Smaller particles (less than 420 μm) contribute most of the flux globally, while larger particles become more important at high latitudes and in tropical upwelling regions. Export from the wintertime mixed layer globally exceeds that from the euphotic zone, suggesting shallow particle recycling and net heterotrophy in the deep euphotic zone. These estimates open the way to fully three-dimensional global reconstructions of particle fluxes in the ocean, supported by the growing database of *in situ* optical observations.

1 Introduction

At the ocean surface, primary production and other biogeochemical processes interact to form organic particles that drive the ocean's biological pump (Volk & Hoffert, 1985; Honjo et al., 2008; Turner, 2015; Siegel et al., 2022). Aggregation and sinking of particulate organic matter stores inorganic carbon and nutrients in the deep ocean for timescales ranging from decades to centuries (DeVries et al., 2012; Boyd et al., 2019), reducing surface carbon concentrations and leading to a decrease in atmospheric CO_2 (Kwon et al., 2009). Sinking particles provide organic matter sustaining the deep ocean biosphere (Robinson et al., 2010) and shape the ocean's microbiome (Karl et al., 1984; Fontanez et al., 2015; Bianchi et al., 2018).

Export of particulate organic matter results from the interaction of complex physical and biological processes (Turner, 2015; Boyd et al., 2019; Siegel et al., 2022). Gravitational settling of particles denser than seawater, including fecal pellets, phytodetritus, and heterogeneous aggregates, is thought to be the primary export mechanism, contributing to about 60% of the total carbon export, and more than half of the carbon storage in the deep ocean (Boyd et al., 2019). Other export processes, such as organic matter transport and repackaging by vertically migrating organisms (Longhurst et al., 1990; Steinberg et al., 2000; Bianchi et al., 2013) and physical injection (Carlson et al., 1994; Omand et al., 2015; Stukel et al., 2017; Dall'Olmo et al., 2016), make up the remainder (Boyd et al., 2019). The importance of large sinking particles in driving the export flux has been well described (Honjo et al., 2008; A. L. Alldredge & Gotschalk, 1988; Turner, 2015), although several studies have also highlighted the importance of smaller aggregates (Alonso-González et al., 2010; Durkin et al., 2015; Kiko et al., 2017; Richardson, 2019).

Export fluxes can be quantified at different depth horizons, with the euphotic zone and mixed layer depths as common choices, underlying competing interpretations: export from the euphotic zone provides an ecosystem-level viewpoint, while export from the mixed layer provides an estimate of long-term carbon storage. Observational and model-based estimates generally evaluate export at the base of the euphotic zone, as defined by the 1% or 0.1% light levels (K. O. Buesseler & Boyd, 2009; Siegel et al., 2014; K. O. Buesseler et al., 2020). On annual timescales or longer, organic carbon export balances net community production (Emerson, 2013), and, since synthesis of new particles is greatly

reduced below the euphotic zone, it also provides an upper limit to the energy that can fuel subsurface ecosystems. Meanwhile, carbon exported below the maximum mixed layer depth is removed from contact with the atmosphere for timescales longer than a year, and thus is relevant for ocean carbon sequestration. Recent work with a global biogeochemical model indicates that the magnitude and patterns of carbon export are sensitive to the choice of depth horizon (Palevsky & Doney, 2018). However, tests of this sensitivity based on global observations are missing.

Because of its central role in ocean biogeochemistry, the global particle export has received significant attention, resulting in a wide range of estimates – from less than 3 to more than 10 PgC y^{-1} (Henson et al., 2011; Siegel et al., 2014; DeVries & Weber, 2017; Dunne et al., 2007), with some of the discrepancies depending on the methods used (Quay et al., 2020). Biogeochemical models yield a global export of 4-6 PgC y^{-1} when tuned to match particle flux observations (Siegel et al., 2014), but can reach up to 10 PgC y^{-1} when tuned to match *in situ* profiles of nutrients and other biogeochemical tracers (DeVries & Weber, 2017). A similar range is suggested by recent global IPCC-class Earth System Models, which produce global carbon exports from 2.4 to 12 PgC y^{-1}, with an average of 7.4 PgC y^{-1} (Séférian et al., 2020). Data-driven estimates that combine satellite-based primary production with empirical measures of particle export ratios often result in fluxes near the upper range (Dunne et al., 2007; Laws et al., 2011; Guidi et al., 2015), with some exceptions (Henson et al., 2011).

A global export of around 10 PgC y^{-1} is comparable to biogeochemical estimates of annual net community production in the mixed layer (Emerson, 2013; Quay et al., 2020). However, on long timescales, community production must be balanced by multiple export processes (Boyd et al., 2019; Siegel et al., 2022) that also include subduction of non-sinking organic carbon (Carlson et al., 1994; Dall'Olmo et al., 2016) and export via vertical migrations of zooplankton and fish (Longhurst et al., 1990; Steinberg et al., 2000; Bianchi et al., 2013). Using an euphotic viewpoint, and considering only gravitational settling, particle flux estimates have begun to converge on a value of 6 PgC y^{-1}, although with significant uncertainty (Boyd et al., 2019).

In the field, sediment traps and thorium-234 measurements have been used to quantify sinking particle fluxes. However, both types of observations lack detailed particle size information, vertical resolution, and have known biases, making extrapolations to global scales difficult (K. Buesseler et al., 2007; Le Gland et al., 2019). Recently, optical methods have gained traction to estimate particle export. These methods are based on *in situ* observations of particle size distribution (PSD), i.e., the number of particles, or abundance, as a function of size (Guidi et al., 2008; Bourne et al., 2019). Among optical instruments, the Underwater Vision Profiler 5 (UVP5) measures the abundance of particles in the 80 μm - 2.6 cm range (Picheral et al., 2010) and is routinely deployed on oceanographic expeditions (Kiko et al., 2022). The high vertical resolution of UVP5 observations, combined with empirical, size-dependent relationships for carbon content and sinking speed (Kriest, 2002; Stemmann et al., 2004; Guidi et al., 2008), enables a uniquely detailed view into the three-dimensional ocean particle flux (Guidi et al., 2016). Observations from UVP5 have been used to quantify particulate fluxes from the surface ocean on a regional basis (Kiko et al., 2017; Cram et al., 2018; Forest et al., 2012), and to reconstruct carbon export across large-scale biomes based on limited sets of measurements (Guidi et al., 2015).

The growing number of UVP5 observations, their global distribution, high vertical resolution, and ability to resolve multiple particle size classes offer an unprecedented opportunity to re-evaluate global carbon fluxes from the ocean's surface, testing the importance of the choice of depth horizon, the role of small vs. large particles, and the degree of autotrophy (i.e., net particle production) vs. heterotrophy (i.e., net particle consumption) across the euphotic zone. In this study, we use a global reconstruction of PSDs from UVP5 observations (Clements et al., 2022) to provide a new estimate of the mag-

nitude and patterns of particulate carbon export from the ocean's surface. The approach relies on empirical relationships that relate particle size and abundance to sinking fluxes (Kriest, 2002; Guidi et al., 2008; Kiko et al., 2017), which we tune against a global data set of *in situ* sediment trap and thorium-derived particle flux observations (Bisson et al., 2018). We exploit the high vertical resolution of UVP5 measurements to estimate particle export at both the climatological euphotic zone depth and the maximum mixed layer depth, elucidating the importance of the export horizon for net carbon export and sequestration.

The rest of the paper is organized as follows. Section 2 describes the methods used to estimate particle fluxes from global PSD reconstructions and *in situ* observations. Section 3 presents the results of the new export estimates, comparing them to prior work, and discussing the implications, uncertainties, and caveats inherent to our approach. Section 4 summarizes the main findings and future directions.

2 Methods

The flux of particulate carbon (ϕ, $\frac{mgC}{m^2 day}$) at any given depth can be expressed as a function of three size-dependent quantities: the number (#) of particles of a given size, i.e., the PSD ($n(s)$, $\frac{\#}{m^3 cm}$), the sinking speed ($w(s)$, $\frac{m}{s}$), and the carbon content of each particle ($c(s)$, $\frac{mg}{\#}$), according to the following equation (Guidi et al., 2008; Stemmann & Boss, 2012):

$$\phi = \int_{s_{min}}^{s_{max}} n(s) \cdot w(s) \cdot c(s)\, ds, \tag{1}$$

Here, s (cm) indicates the particle ESD, or size, and s_{min} and s_{max} the minimum and maximum size of particles considered for export. Following previous work, we assume that the quantities in Equation 1 can be approximated by power laws that depend on particle size, each characterized by an intercept (the size-independent coefficient) and a slope (the exponent for size-dependence) (Stemmann & Boss, 2012):

$$n(s) = n_0 \cdot s^{-\beta} \tag{2}$$

$$w(s) = w_0 \cdot s^{\eta} \tag{3}$$

$$c(s) = c_0 \cdot s^{\zeta}, \tag{4}$$

Thus, by using Equations 2-4, the total particle flux can be expressed as:

$$\phi = \int_{s_{min}}^{s_{max}} n_0 \cdot w_0 \cdot c_0 \cdot s^{-\beta+\eta+\zeta}\, ds = \int_{s_{min}}^{s_{max}} n_0 \cdot m_0 \cdot s^{-\beta+\mu}\, ds \tag{5}$$

where we combined the intercepts and exponents of the sinking speed and carbon content relationships by setting $m_0 = w_0 \cdot c_0$ and $\mu = \eta + \zeta$, following the approach by Guidi et al. (2008). We further approximate m_0 and μ with globally constant values, which we constrain with *in situ* observations. In practice, we calculate the continuous integral in Equation 5 as a discrete summation over the finite size bins that approximate the PSD observed by UVP5 instruments.

We use PSD properties (biovolume and slope) from a global UVP5-based reconstruction, shown in Figure 1 (Clements et al., 2022). Briefly, this reconstruction is based

on a machine learning algorithm (a bagged Random Forest ensemble) applied to a global dataset of UVP5 observations (Kiko et al., 2022), and provides monthly varying climatological maps of PSD slope and biovolume in the upper ocean. We combine these PSD reconstructions with empirical relationships for sinking velocity and carbon content to estimate particle fluxes by solving Equation 5. Since the parameters that define the combined sinking speed and carbon content relationships, i.e., m_0 and μ, are poorly constrained (Kriest, 2002; Stemmann & Boss, 2012; Kiko et al., 2017), we optimized them by minimizing the mismatch between predicted particle fluxes and *in situ* observations from sediment traps and thorium-uranium disequilibrium at the base of the euphotic zone (Bisson et al. (2018), see Section 2.1).

We exploit the three-dimensional nature of UVP5 observations to calculate particle fluxes at two different export horizons: the base of the euphotic zone (here defined by the 1% light level following Morel et al. (2007)) and the annual maximum mixed layer depth (Johnson et al., 2012). For the former, we take the PSD estimates from Clements et al. (2022). For the latter, we estimate the PSD at the base of the wintertime mixed layer, following the same procedure as Clements et al. (2022).

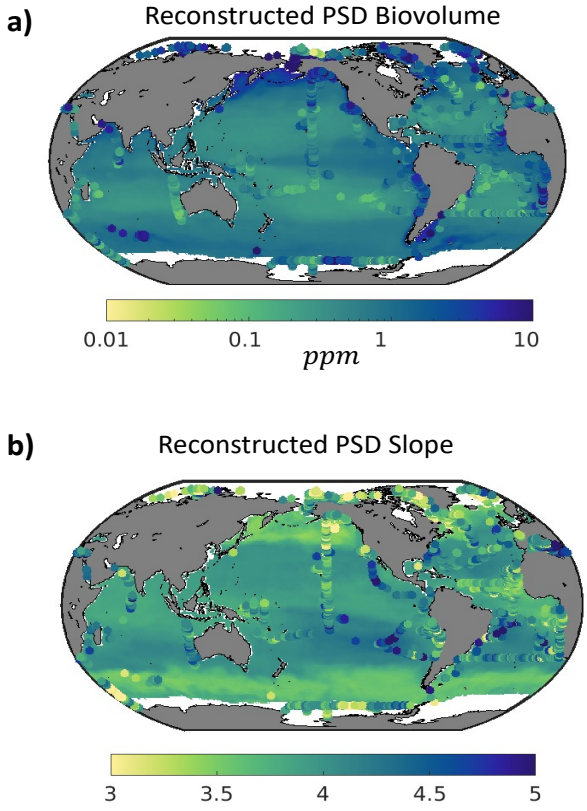

Figure 1. Global reconstructions of (a) PSD biovolume (ppm), and (b) PSD slope (non-dimensional), based on a machine-learning extrapolation of *in situ* UVP5 observations (Clements et al., 2022). Color contours show reconstructed variables as annual means. Dots show *in situ* quantities from UVP5 observations. Note that observations reflect specific months of the year, explaining some of the mismatches with annual mean quantities shown by the background colors.

2.1 Sinking Speed and Carbon Content

Particle sinking speed and carbon content have been empirically evaluated using power law relationships analogous to Equations 3 and 4, e.g., as compiled in Kriest (2002) and Stemmann et al. (2004). Individually, most observational studies measure a range of particles that does not wholly encompass the sizes detected by the UVP5. Furthermore, these relationships are defined for specific particle types, which are not distinguished in the PSD reconstruction used here (Clements et al., 2022).

Since estimates of total flux are sensitive to the sinking speed and carbon content relationships encapsulated by the parameters m_0 and μ, we apply an optimization procedure to keep our results consistent with *in situ* particle flux measurements. Specifically, we find the values of m_0 and μ that minimize the sum of the square errors between the log of the particle flux reconstructions (Equation 1) and co-located *in situ* carbon flux measurements (Bisson et al., 2018). We use both trap and thorium flux data, corrected to be at the euphotic depth. We average together all *in situ* data onto the same grid of the PSD reconstructions (Clements et al., 2022), i.e., into 1 degree grids, by month, so that the optimizations are done on a climatological basis. Because *in situ* carbon flux measurements are uncertain (Bisson et al., 2018), we adopt a Monte Carlo approach for this optimization, repeating it 1000 times after perturbing each flux observation by applying a random observational error, assuming a log-normal distribution and an uncertainty of 1 standard deviation on the measurements. This Monte Carlo ensemble also allows us to estimate the error associated with the optimization of the sinking speed and carbon content parameters.

Because the size distribution of particles that contribute to the flux is poorly constrained, we perform this optimization for a range of plausible minimum and maximum sizes for Equation 5, selecting a physically reasonable combination for the final estimate. Ultimately, when optimizing the sinking carbon parameters, the total global export flux is not sensitive to the size range; however the resulting empirical relationships are. The insensitivity of the carbon flux to the size range indicates a compensatory effect between the sinking carbon parameters and the size range selected for the optimizations. Thus, choosing different size combinations would result in a similar total flux, although it may slightly alter spatial or temporal patterns in a compensatory way (SI Fig. 1).

Our final choice of size range is informed by average sinking speeds and carbon content previously reported (Kriest, 2002). Based on this optimization analysis, we set the minimum size class to be 35 μm, where the average sinking speed is near 1 m d^{-1} (Smayda, 1970; Kriest, 2002). Although this value is lower than the detection limit of the UVP5, the power law slope can likely be extended to this size range, as demonstrated for example by observations in the the Pacific Ocean (Stemmann, Eloire, et al., 2008). Most organic particles smaller than this size are likely rapidly remineralized, making their contribution to the sinking flux negligible (Riley et al., 2012). Even if some smaller particles could sink more rapidly (e.g., because of higher concentrations of mineral "ballast" and higher density) and could contribute more substantially to the total flux, neglecting them would not significantly affect our final export, because the optimized flux is nearly insensitive to the size range selected (SI Fig. 1). We choose 5 mm as the maximum size, i.e., the same maximum size used for the PSD reconstructions (Clements et al., 2022), roughly corresponding to the size where zooplankton become important contributors to the particle biovolume detected by UVP5 in a variety of regions (Forest et al., 2012; Stemmann, Youngbluth, et al., 2008; Stemmann & Boss, 2012).

Overall, this optimization approach results in a median value of 2.63 $\pm$ 0.06 for the exponent μ, and 18.0 $\pm$ 2.8 mgC m s^{-1} $cm^{-2.63}$ for the intercept m_0, both in the range suggested by *in situ* observations (Kriest, 2002), and comparable to values adopted by previous studies (Kriest, 2002; Stemmann et al., 2004; Guidi et al., 2008; Kiko et al., 2017; Bianchi et al., 2018).

2.2 Flux reconstruction, error and evaluation

We first present results for fluxes estimated at the climatological euphotic zone depth, and then repeat the calculation at the maximum mixed layer depth. This requires an estimate of the PSD at the maximum mixed layer depth, which we obtain from UVP5 observations following the same machine learning approach of Clements et al. (2022). We keep the same sinking speed and carbon content parameters (m_0 and μ), assuming that they do not change substantially between the two depths, which are often not too far apart from each other. Thus, the only methodological difference between the two estimates is the depth of the PSD reconstruction used to calculate the flux.

We take the ensemble mean of the Monte Carlo optimizations (Section 2.1) as the final carbon flux estimate. Error in this estimate could arise not only from the uncertainty in the particle sinking speed and carbon content parameters, but also from the uncertainty in the PSD reconstructions (Clements et al., 2022). We combine these two sources of error by summing the variances of two ensembles of carbon flux reconstructions. The first consists of the Monte Carlo optimization ensemble, based on the mean PSD from Clements et al. (2022). The second uses 100 different realizations of PSD from Clements et al. (2022), but sets m_0 and μ to the median values from the optimization. The final uncertainty is taken as the square root of the combined variances.

We evaluate reconstructed particle export fluxes by comparing them to *in situ* flux observations and previous global reconstructions. Specifically, we compare total fluxes, zonal averages, and seasonal cycles. For these comparisons, we divide the ocean into 14 biogeochemically consistent regions based on the boundaries identified by Weber et al. (2016), with an additional boundary along the equator to separate Northern and Southern Hemispheres.

3 Results and Discussion

3.1 Euphotic zone export fluxes

Our resulting global carbon flux reconstruction at the base of the euphotic zone compares well with *in situ* sediment trap and thorium-based observations (Fig. 2), performing in a similar way as previous estimates (Henson et al., 2011; Dunne et al., 2007; Siegel et al., 2014). Compared to previous work, we reduce the uncertainty relative to observations, as expressed by the lower root mean square error and bias. However, our method also reduces the full range of reconstructed fluxes, i.e., it overestimates the flux at low values and underestimates it a high values compared to observations. This bias could be related to a similar underestimate of the range of PSD biovolume and slope that likely depends on the specific machine learning method used to extrapolate UVP5 observations (Clements et al., 2022). It is also possible that the optimization approach against an averaged global dataset of *in situ* fluxes fails to capture extremes in particle export at both the high and low range of observations.

Comparing sediment trap and thorium-based observations to the various estimates of Fig. 2 highlights the relative strengths and weaknesses of each approach. The results from Dunne et al. (2007), based on combining satellite primary production with empirical estimates of particle export ratios, match the observed values well, but tend to overestimate the largest fluxes (not shown on these figure axes). The estimate by Henson et al. (2011), based on a similar approach as Dunne et al. (2007), follows a similar pattern as observations, as indicated by the high r^2, but systematically underestimates the flux magnitude, as shown by the negative bias. The satellite-driven, model-based estimate from Siegel et al. (2014) captures the overall magnitude of export, but misses some of the variability of observations, as indicated by the relatively low r^2. Overall, all estimates in Fig. 2 show combinations of strengths and weaknesses, and it would be difficult to highlight a specific model as unconditionally superior. This suggests that a combination of

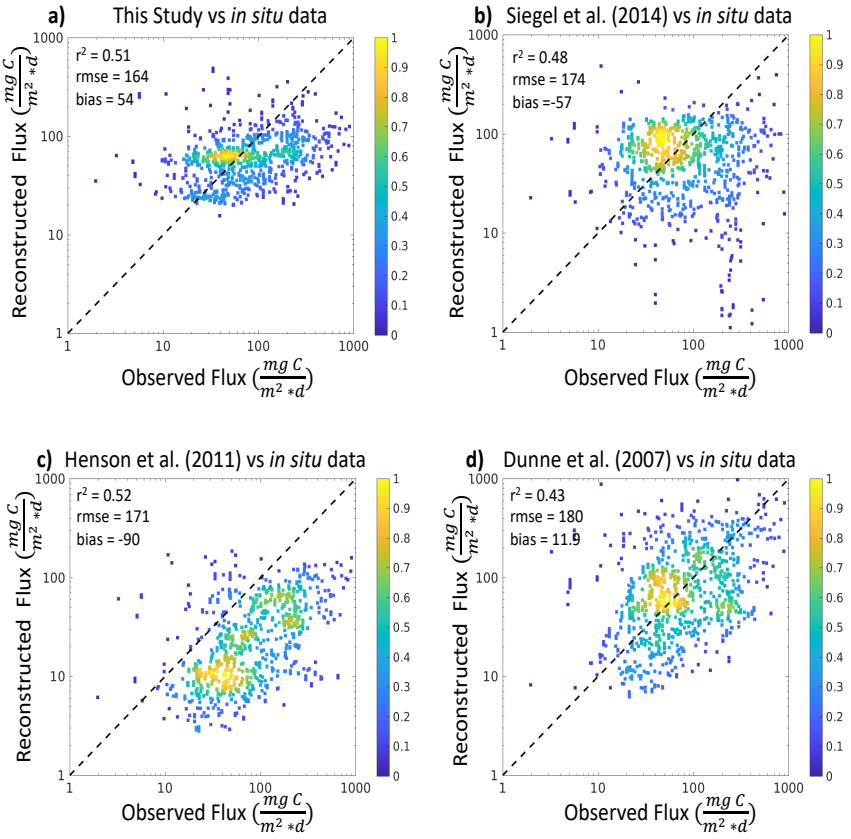

Figure 2. Density scatter plots showing the relationships between *in situ* flux observations and global flux reconstructions (mg C m^{-2} d^{-1}) at the base of the euphotic zone from (a) this study, (b) Siegel et al. (2014), (c) Henson et al. (2011), (d) (Dunne et al., 2007). Colored dots represent the relative density of grid points surrounding the data point, and the dashed line indicates a 1:1 ratio. Annotations show the coefficient of determination (r^2), root mean square error (RMSE), and average bias. Note that to keep similar x-axes and allow better comparison between the different estimates, a limited number of points with flux larger than 1000 mg C m^{-2} d^{-1} have been omitted from the figures.

estimates should be used to asses export of carbon from the surface ocean, and that future efforts should strive to reduce the biases discussed above, potentially combining strengths from different approaches.

Extrapolated to the whole ocean, our method reveals spatial patterns of export fluxes in broad agreement with previous studies, with some notable differences (Fig. 3). Similar to other estimates, particle fluxes tend to decrease from high to low latitudes, and from coastal regions to the open ocean. A local maximum of export is reproduced along the equator, and is particularly evident in the Pacific Ocean. Compared to previous work, our method produces somewhat weaker gradients between coastal and offshore waters, with slightly higher fluxes near the centers of subtropical gyres, and suggests an asymmetry between the subpolar Atlantic and Pacific Oceans, with more intense particle export along the gulf of Alaska than in the North Atlantic (see also Section 3.1.1). We also reconstruct substantially stronger export than previously found in the Southern Ocean, in particular south of 50S (see discussion in Section 3.2).

Globally integrated, we estimate a particle export flux of 5.8 ± 0.1 PgC y^{-1}, in good agreement with the range of observational and model-based estimates of the biological gravitational pump (4-9 PgC y^{-1}, Boyd et al. (2019)). Compared to other spatially resolved reconstructions, our global flux sits between the low-value of Henson et al. (2011) (3.0 ± 0.3 PgC y^{-1}) and the high-value of Dunne et al. (2007) (8.5 ± 0.81 PgC y^{-1}). Seasonal maps of the export and standard deviation are shown in Supplementary Figures S2 and S3.

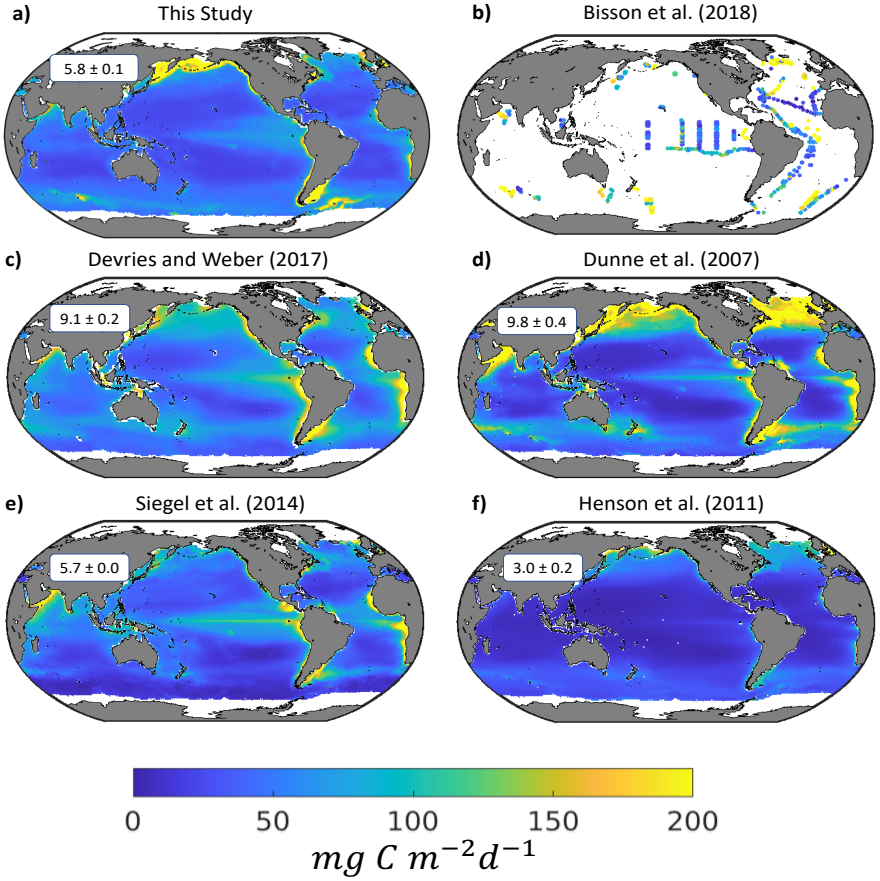

Figure 3. Annual average particle export flux (mg C m^{-2} d^{-1}) from the euphotic zone for (a) the global PSD-derived flux from this study, compared to (b) the *in situ* data of Bisson et al. (2018), (c) the steady state satellite-driven model SIMPLE-TRIM of DeVries et al. (2017), (d) the empirical model of Dunne et al. (2007), (e) the satellite-driven euphotic zone food web model Siegel et al. (2014), and (e) the empirical model of Henson et al. (2011). Annotations in each figure show the globally integrated export in Pg C y^{-1}, and the uncertainty reported by each study.

3.1.1 Spatial variability

Variations in export patterns derived with our approach (Equations 1 and 5) reflect a combination of spatially varying PSD biovolume and slope (Clements et al., 2022). We can quantitatively describe the effect of the PSD as the relative contribution of small (35 μm - 418 μm) vs. large particles (418 μm - 5 mm) to the total flux (Figure 4), where 418 μm is the geometric mean of the size range considered here. Biovolume and PSD slope generally correlate in such a way that both factors contribute to increasing export fluxes

in particle-rich productive waters, where large, rapidly sinking particles tend to be relatively more abundant than small particles, and to decreasing export fluxes in particle-poor oligotrophic waters where small particles dominate (Clements et al., 2022) (Figure 4).

High export in the eastern equatorial and tropical Pacific can be attributed to high biovolume, with a minor contribution from PSD slope, which appears to be more uniform across the region (Figure 1). The picture is somewhat different in the equatorial Atlantic Ocean, where a more substantial "flattening" of the PSD supports a higher contribution from large particles. A similar interaction of particle abundance and size-structure dramatically intensify fluxes at high latitudes, such as in the subpolar North Pacific and Southern Ocean, and to a lesser extent the subpolar Atlantic, where an increase in particle abundance is accompanied by a shift of the PSD toward large particles. In contrast, along many coastal regions, including eastern boundary upwelling systems and the Arabian Sea upwelling, increase in particle biovolume, rather than substantial changes in size structure, appears to drive enhanced export fluxes. We speculate that changes in community structure associated with more productive regions explain such a shift.

We illustrate the main spatial differences between our and other reconstructions by considering zonally averaged export fluxes (Fig. 5). The largest export rates are observed around the equator, in the subpolar Pacific Ocean, and in the mid- to high-latitudes of the South Atlantic Ocean, while more uniform export is observed in the Indian Ocean. In all basins, the minimum export rates are generally located at the latitude of the subtropical gyres. While export is nearly symmetrical around the equator in the Pacific Ocean (Fig. 5a), in the Atlantic Ocean it dramatically increases moving from the Northern to the Southern Hemisphere (Fig. 5b). These patterns reflect a combination of open-ocean and shelf enhanced particle fluxes. Specifically, high export in the Northern Pacific and Southern Atlantic Oceans are partly driven by large fluxes in the Bering Sea, the Sea of Okhotsk, and the Patagonian shelf. At lower latitudes, coastal upwelling systems sustain particularly high export in the northern Indian Ocean and the tropical to subtropical Atlantic.

Our reconstruction shows broad meridional patterns similar to previous estimates (Fig. 5); however, significant regional-level discrepancies remain. For example, in the low latitudes, we predict somewhat less intense equatorial export peaks and subtropical lows, compared to the estimates of Dunne et al. (2007) and Siegel et al. (2014). In this respect, our reconstruction is more in line with that of DeVries and Weber (2017). In the northern Pacific, we do broadly underestimate the transition zone as a persistent feature; however, seasonally, it is present (Supplementary figure S2). Overall, in the subpolar North Pacific, our estimate shows a northward shift of maximum export towards the continental margins that is comparable to the results of Dunne et al. (2007). This is likely caused by intensification of particle fluxes in coastal waters and marginal seas, which may be related to regional processes such as more efficient nutrient recycling in shallow regions, or iron leakage from continental shelves (Nishioka et al., 2020) supporting large phytoplankton sizes. In the Atlantic Ocean, the gradual increase of export from northern to southern latitudes (mostly driven by high export near the coast), and the rapid increase in the Southern Ocean (caused by high export near the Patagonian shelf), are similar to the reconstruction of Henson et al. (2011), although the magnitude is larger. In the Indian Ocean, our reconstruction matches other studies at low latitudes; however, it shows a more dramatic increase in export towards the Southern Ocean sector (discussed in more detail in Section 3.2).

3.1.2 Seasonal cycle

The seasonal cycle of particle export is comparable to previous studies, when averaged over large-scale coherent biomes (Fig. 6). However, significant discrepancies are

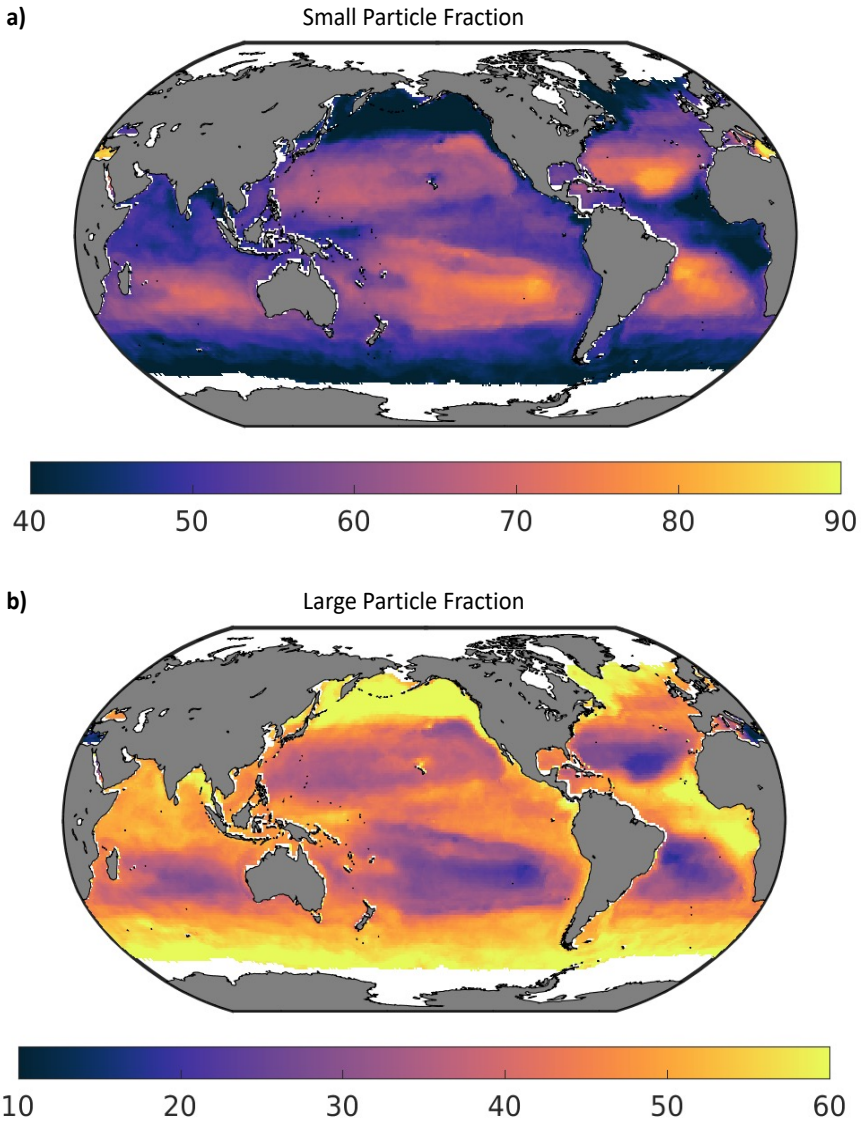

Figure 4. Role of small vs. large particles. The two panels show the fraction of carbon flux at the euphotic zone from (a) small particles ($35\mu m$ to $418\mu m$ ESD) and (b) large particles ($418\mu m$ to $5mm$ ESD).

also revealed. In general, our seasonal cycle is more muted than previous work, suggesting weaker month-to-month variability in some regions, while other regions match previous reconstructions more closely. The most significant discrepancy is observed in the Southern Ocean, in particular in the Antarctic zone, where our reconstruction is substantially higher than previous estimates, with sustained export throughout winter months. We discuss this deviation in Section 3.2.

The lower seasonality in our estimate is consistent with the reduced spatial gradients, and suggests overall weaker variations in net community production and export than previously assumed. The machine learning approach used to reconstruct the PSD relies on non-linear relationships with multiple ocean variables to reconstruct particle

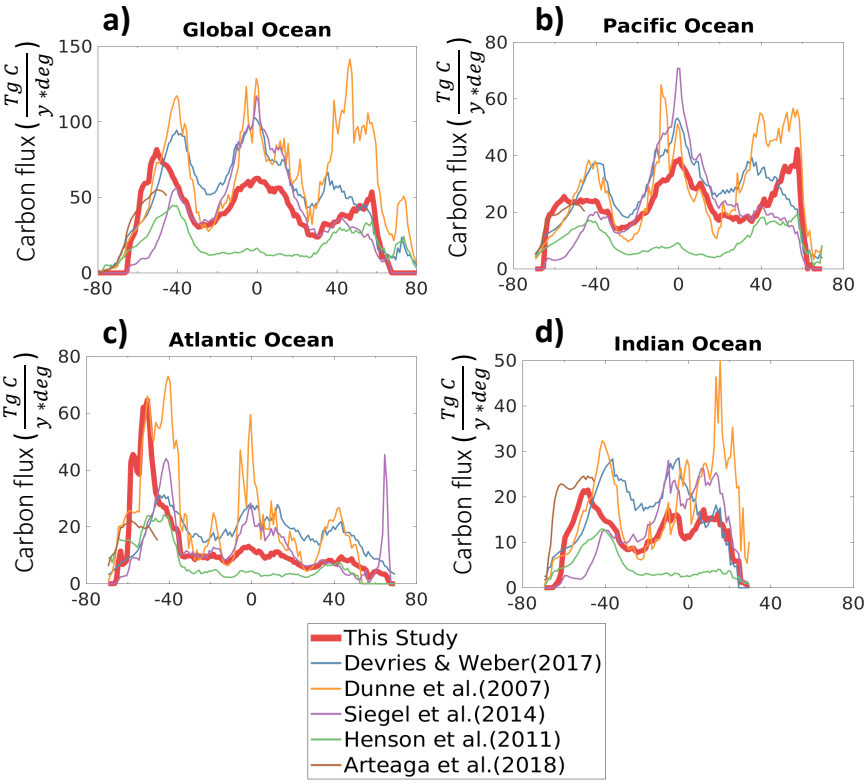

Figure 5. Zonally integrated annual mean export (Tg C y^{-1} $degree^{-1}$) from the base of the euphotic zone, for (a) the Global Ocean, (b) the Pacific Ocean, (c) the Atlantic Ocean, and (d) the Indian Ocean. Each color represents a different study, as shown in the legend (bottom).

size distributions, which may accentuate compensatory relationships between different predictors. Surface chlorophyll, temperature, and net primary production have all been used in previous global reconstructions (Dunne et al., 2007; Henson et al., 2011; Siegel et al., 2014), but rarely together with additional variables that may be important in modulating spatial and seasonal patterns of export. It is also possible that our method somewhat underestimates variability compared to previous work. As previously noted, our PSD reconstructions reduces extremes in both biovolume and PSD slope (Clements et al., 2022), which may lead to underestimating variability in particle export fluxes derived from these quantities.

3.2 Southern Ocean Export

Export flux in the Antarctic zone of the Southern Ocean are larger in our estimate than other global reconstructions, especially during austral summer (Fig. 6). We also find a southward shift in export, with a peak around 50S, rather than around 40S as in other estimates. A regional study based on 10 years of biogeochemical Argo measurements from 2006-2014, combined with satellite-based net primary production and export algorithms, similarly suggests higher than previously reported particle fluxes throughout the region (Arteaga et al., 2018), in better agreement with our results (Fig. 7). This similarity is mostly evident in the open ocean, and varies depending on the primary production algorithm chosen for the comparison. However, our estimate also suggests substantially higher export near landmasses, for example South Georgia and the South Sandwich Islands and the Kerguelen Plateau. Although estimates from Arteaga et al. (2018)

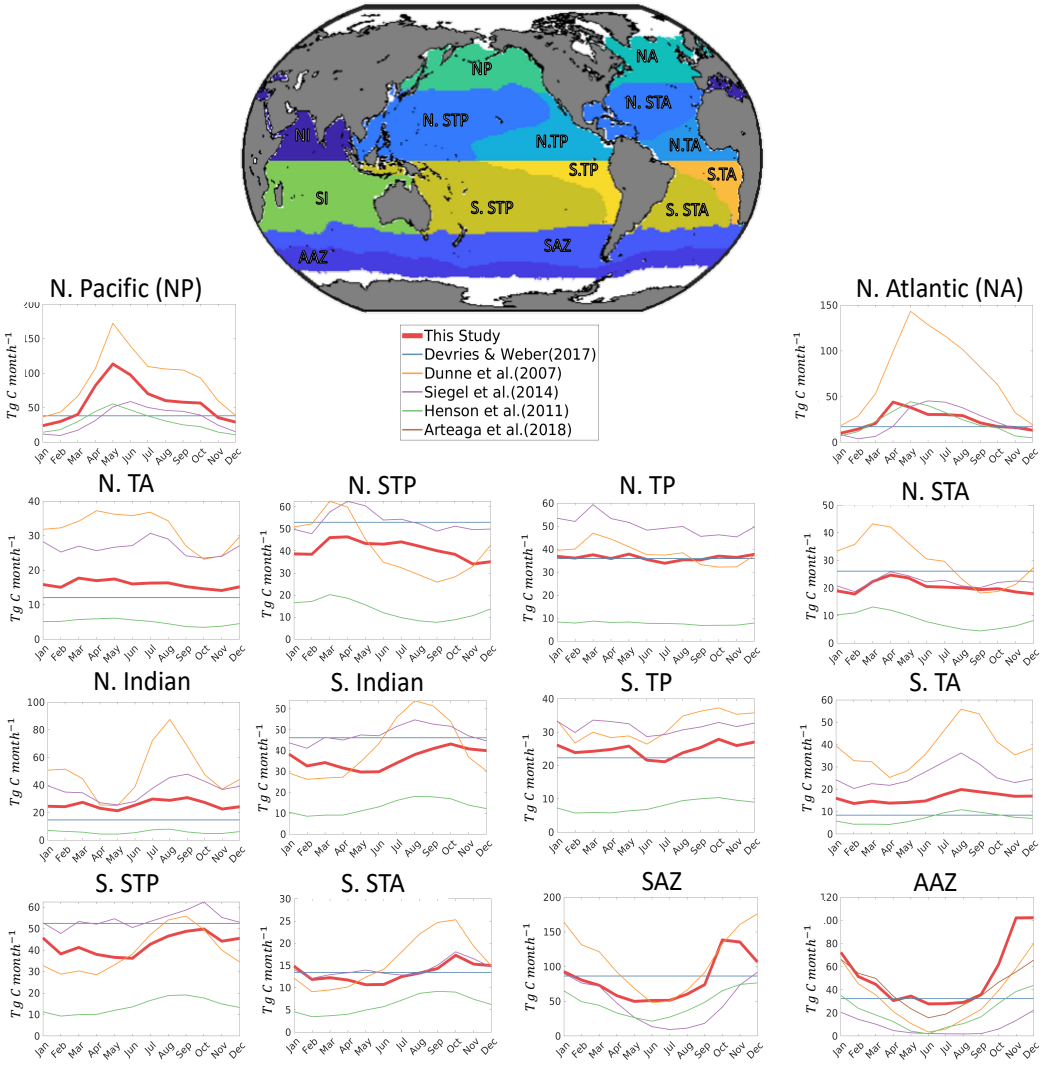

Figure 6. Annual seasonal cycle of particle flux from the euphotic zone (Tg C y^{-1}) for the regions specified in the map (top). Each line corresponds to a different estimate, as listed in the legend below the map. The same seasonal spatial mask was applied to each study. Note that the study by DeVries and Weber (2017) provides annual mean export fluxes, which are shown here as horizontal lines.

do not show the same high flux in austal winter through the end of the year as our reconstruction, they do demonstrate that export fluxes from the Antarctic zone of the Southern Ocean likely never decrease to the nearly negligible levels shown by other global estimates (Fig. 6).

The discrepancy in export from the Antarctic zone relative to prior global estimates could arise from a combination of factors. Observations in the Southern Ocean, particularly in austral winter, are scarce. This is true for both the UVP5 measurements and the climatological predictors used to reconstruct PSD (Clements et al., 2022). The UVP5 data compilation (Kiko et al., 2022) includes two major cruises in the Southern Ocean, which only cover the months of March to May. Satellite-based reconstructions of chlorophyll and primary production from ocean color are on the other hand poorly resolved

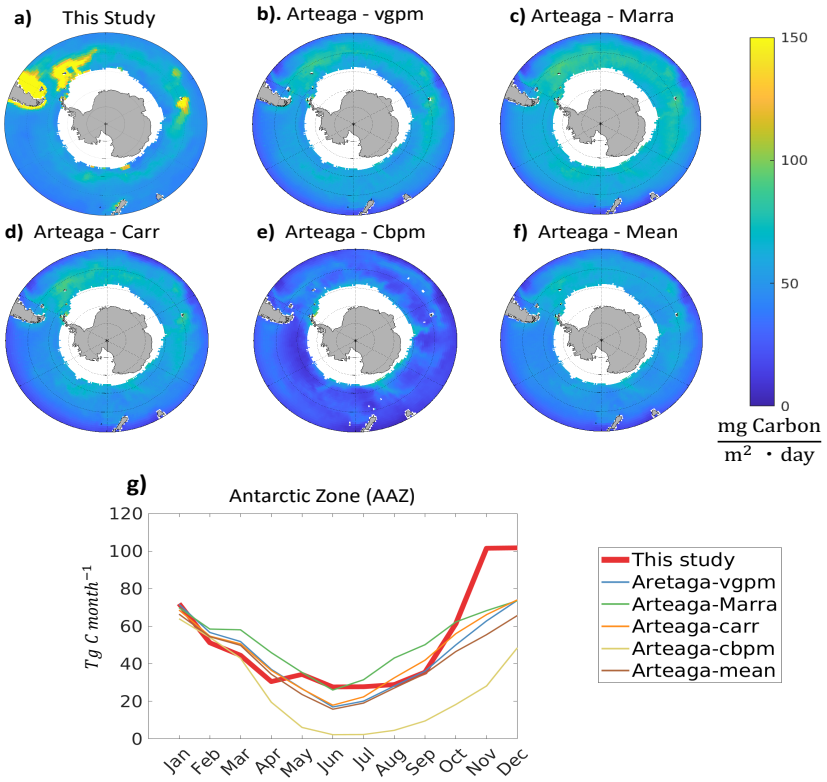

Figure 7. Southern Ocean particle export (mg C m^{-2} d^{-1}) for (a) this study, and (b-e) different data-based estimates from Arteaga et al. (2018), and (f) the mean from that study. Each data-based estimate from Arteaga et al. (2018) uses a different net primary production algorithm to derive export. (g) Seasonal cycle of export for each estimate in the Antarctic zone (shown in figure 6).

in austral wintertime. Other climatological variables, such as nutrients and oxygen, are also the results of interpolation of fewer *in situ* observations relative to the rest of the ocean. The scarcity of observations to train the machine learning model used for the PSD reconstructions results in significant uncertainty in predicted PSD and export fluxes in this region (Clements et al., 2022).

Our reconstruction reveals significant export primarily next to island masses. Proximity to Southern Ocean islands have been shown to increase productivity and carbon flux (Jouandet et al., 2014; Stemmann, Eloire, et al., 2008), presumably via enhanced vertical mixing and iron fertilization from sedimentary sources in otherwise high-nutrient low-chlorophyll waters (Gaiero et al., 2003). It is possible that other methods of flux reconstructions (Henson et al., 2011; Siegel et al., 2014; DeVries & Weber, 2017) underestimate this increased export, in particular during winter, when observations are scarce. Expanding the number of *in situ* particle flux and UVP5 observations from the Antarctic zone, downstream of major land masses and over the entire seasonal cycle, could help shed light on the patterns of export and their variability in this undersampled region.

3.3 Mixed layer versus euphotic zone export

Globally integrated, export from the maximum wintertime mixed layer depth is 6.1 $\pm$0.1 PgC y^{-1}, i.e., about 0.5 PgC y^{-1} larger than the global export from the euphotic

zone. This estimate is lower than observational estimates of organic carbon export and annual net community production from the same depth horizon (Emerson, 2013), which would include additional export mechanisms.

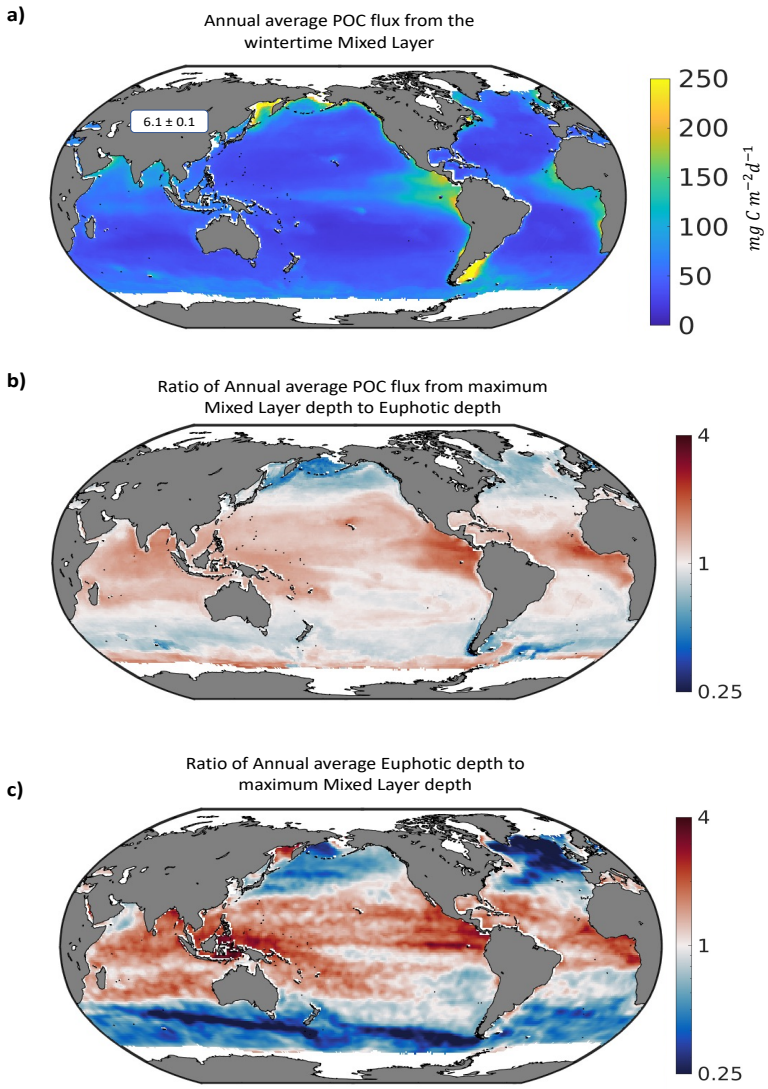

Figure 8. (a) Annual mean particle export (mg C m^{-2} d^{-1}) from the maximum mixed layer depth. Total export is 6.1 PgC y^{-1}. (b) Ratio of the export from the MLD to the export from the Euphotic zone. Red indicates a higher export from the MLD (c) Ratio of the annual mean Euphotic zone depth to the Maximum annual mixed layer depth. Red indicates where the euphotic zone is deeper.

Overall, export from the wintertime mixed layer follows broad spatial patterns similar to the export from the euphotic zone (Fig. 8a). The tropics and subtropics show larger mixed layer export fluxes (locally, up to a few times), while high latitudes show overall weaker values (Fig. 8b). The low-latitude intensification of mixed layer fluxes is similar in all ocean basins, and more than compensates for the reduction at high latitudes (Supplementary Fig. S6), thus producing an overall larger export from this horizon. Because of this low-latitude intensification, export from the mixed layer shows stronger gradients between the tropics and high latitudes. Gradients between the equatorial export

peak and the subtropical export low are also intensified. Finally, export from the mixed layer in the Southern Ocean is substantially depressed compared to export from the euphotic zone. Similar to export from the euphotic zone, export from the mixed layer tends to be dominated by smaller particles (SI Fig. S7)

Differences between euphotic zone and mixed layer export can be best interpreted by considering the different depth of these horizons (Palevsky & Doney, 2018) (Fig. 8 C). The maximum mixed layer is shallower than the euphotic zone in the tropics and sub-tropics, and is deeper in high latitudes (Fig. 8c). This suggests that shallower export horizons are generally characterized by higher fluxes than deeper export horizons, which we attribute to remineralization of particles in surface layers. Specifically, we identify three main latitudinal bands with different horizon depths and export patterns, roughly corresponding to tropics and subtropics, mid-latitudes, and subpolar regions.

Over most of the tropics and the subtropics, the maximum wintertime mixed layer is shallower on average than the climatological euphotic zone (blue colors in Fig. 8 c). Here, particle remineralization between the wintertime mixed layer and the euphotic zone depth likely reduces export from the latter horizon, suggesting net heterotrophy in the deeper layers of the euphotic zone, consistent with observations of shallow particle regeneration in the tropics (Pavia et al., 2019).

Over subpolar regions, the wintertime mixed layer is deeper on average than the climatological euphotic zone. Thus, export fluxes reach maximum values within the euphotic zone, and decrease below it following typical flux attenuation profiles (Martin et al., 1987; Guidi et al., 2009). Finally, over most of mid-latitudes, the wintertime mixed layer is deeper on average than the climatological euphotic zone. However, export fluxes from the mixed layer and euphotic zone are very similar in magnitude, suggesting a close seasonal compensation between enhanced euphotic zone fluxes when this horizon is found above the wintertime mixed layer, and reduced euphotic zone fluxes when it is found below it.

Ultimately, differences in export between the euphotic zone and the wintertime mixed layer are important when considering the role of the biological pump for carbon sequestration (Palevsky & Doney, 2018). Export below the wintertime mixed layer removes carbon from contact with the atmosphere for timescales longer than one year. Our results suggest that more carbon is sequestered below the wintertime mixed layer than leaves the euphotic zone. We further suggest a role for particle consumption by heterotrophes (microbes and zooplankton) in reducing the abundance of organic particles in the lower euphotic zone, making it net heterotrophic rather than primarily autotrophic.

3.4 Caveats to our approach

Our method relies on global PSD reconstructions from UVP5 observations, as well as *in situ* particle flux measurements, both of which are spatially and temporally limited. This in turns reduces the ability of our approach to obtain an accurate climatological picture of PSD and fluxes, and extrapolate local observations to larger regions and other times of the year. In particular, about forty-three percent of monthly particle flux observations contain only one data point, and entire ocean basins are represented by a handful of measurements (Fig. 2b). While more widely distributed than flux measurements, UVP5 observations are also characterized by large gaps in space and time (Kiko et al., 2022).

As previously discussed (Clements et al., 2022), regional correlations between environmental properties and PSD observations from UVP5 may not be well captured by extrapolation with a machine learning algorithm trained on data from different regions, especially when non-linear relationships between variables become important. Similarly, our reconstructions rely on the assumption that PSD can be well approximated by power

law distributions. Analysis of UVP5 data suggest that this assumption is generally valid over the open ocean (Clements et al., 2022), although locally it may be flawed, and other distributions may be more accurate (R. A. Reynolds & Stramski, 2021). Expanding the coverage of *in situ* PSD and fluxes, in particular in under-sampled regions characterized by large variability, such as the Southern and northwest Pacific Oceans, would improve the robustness of our estimates, and shed additional light on regional export patterns not captured by previous work.

The conversion of PSD to export flux encapsulated by Equations 1 and 5 also suffers from limitations. Converting standing stocks of particles from UVP5 observations to sinking carbon flux using size-dependent relationships assumes that (1) all particles of a given size have the same carbon content, and (2) they all sink at a similar speed proportional to their size. Known biases exist with both assumptions. For example, densely packed fecal pellets often contain more carbon and sink faster than heterogeneous aggregates and marine snow of the same size (A. Alldredge, 1998). Biogenic and lithogenic minerals could alter these relationships on a regional basis, e.g., near continental margins, where lithogenic particles are generally more abundant (R. Reynolds et al., 2010; Trudnowska et al., 2020). Furthermore, we assume globally uniform relationships between particle size, sinking speed, and carbon content. However, these relationships remain highly uncertain (A. Alldredge, 1998; Stemmann, Eloire, et al., 2008; Stemmann & Boss, 2012; Cael et al., 2021), and are likely to depend on region and time of the year, reflecting variable particle characteristics and underlying oceanographic and ecological processes.

Our approach, which optimizes carbon content and sinking velocity parameters against *in situ* particle fluxes, reduces to some extent the effect of these uncertainties. More work combining *in situ* and optical measurements should focus on constraining these quantities and their regional and temporal variability. Future studies could also improve our approach by distinguishing living and non-living particles, as well as particle type and composition, e.g., by analysis of UVP5 images or other optical methods in conjunction with *in situ* particle samples (Trudnowska et al., 2021).

4 Conclusions and future work

We provide a new, data-constrained estimate of particle export fluxes by combining global reconstructions of PSD from UVP5 observations and *in situ* export flux measurements. Our estimate of particle export captures regional and seasonal variability in fluxes, and allows reconstruction of export fluxes from spatially variable euphotic zone and mixed layer depths, highlighting the importance of the choice of export horizon (Palevsky & Doney, 2018).

We obtain a global particle export flux of 5.8 ± 0.1 PgC y^{-1} from the euphotic zone, in line with previous work, although with regional and temporal differences. Our results suggest weaker spatial and seasonal variability compared to previous studies, in particular in the open ocean, and highlight the importance of coastal waters and marginal seas for export at high latitudes. Results from the Southern Ocean suggest that processes that sustain elevated fluxes, in particular in wintertime and early austral summer, may not be completely captured by other global reconstructions, and that waters downstream of coasts and islands may harbor a significant source of carbon export to the deep ocean, which is only partially captured in one other reconstruction (Dunne et al., 2007).

We illustrate the ability of our method to obtain particulate organic carbon fluxes at multiple depth by reconstructing and comparing carbon export from the euphotic zone and the wintertime mixed layer depth. Export from the mixed layer is overall stronger than export from the euphotic zone in low and mid latitudes, and weaker in high latitudes, driving a marginally larger flux of 6.1 ± 0.1 PgC y^{-1}. Differences between euphotic zone and mixed layer export are only partially consistent with results from large

scale models (Palevsky & Doney, 2018), and suggest important organic matter remineralization in the deeper parts of the euphotic zone. Three-dimensional reconstructions of particle fluxes would allow a closer investigation of the processes controlling export changes with depth and their implications for particle transfer efficiency and carbon sequestration.

Our results highlight the relative importance of particle abundance and size structure in driving export. Total particle biovolume and the PSD slope are correlated in such a way to act synergistically on particle fluxes (Clements et al., 2022). Consistently, higher fluxes are reconstructed in regions with larger particle biovolume and "flatter" slopes. We also suggest distinct deviations from these patterns, for example in the tropical and northern subtropical Pacific Ocean, where high abundance of all particles, rather than dominance of large relative to small particles, appears to drive elevated export. We further highlight the importance of the PSD by comparing export for small and large particles (here separated at a cutoff size of 418 μm), showing that, while small particles (35 μm - 418 μm range) overall dominate export, large particles (418 μm - 5 mm range) become proportionally more important in high latitudes and tropical regions, where they can account to up to 60 % of export fluxes.

We identify sources of uncertainty and limitations that should be addressed in future work. There remain areas of the ocean and times of the year with limited UVP5 observations and, critically, *in situ* flux measurements, driving uncertainty in both the PSD and flux reconstructions. As UVP5 observations increase in number, our analysis can be refined, for example by expanding comparison with *in situ* sediment trap and thorium-based particle flux observations (Mouw et al., 2016). New machine learning approaches should aim at better capturing fluxes at the high and low end of their range, reducing current biases (Clements et al., 2022). Furthermore, better constraints should be placed on particle carbon content and sinking speed parameters, reflecting regional variability and particle types.

The three-dimensional nature of UVP5 observations paves the way for fully three-dimensional reconstructions of particle export fluxes in the ocean interior. This will greatly benefit from particle flux compilations that span the full depth of the ocean (Mouw et al., 2016), and that harmonize discrepancies between different flux measurement methods (Bisson et al., 2018). Ongoing deployments of UVP instruments, including on Argo floats, will rapidly increase the number of PSD observations with high vertical resolution (Picheral et al., 2022). In turn, three-dimensional reconstructions of export will enable a better characterization of the ocean's ability to sequester carbon (Boyd et al., 2019), and, in combination with models (DeVries & Weber, 2017; Siegel et al., 2014), a better understanding of the processes behind the ocean's biological pump (Siegel et al., 2022).

Acknowledgments

This material is based upon work supported by the U.S. National Science Foundation under grants No. OCE-1635632 and OCE-1847687. D.B. acknowledges support from the Alfred P. Sloan Foundation, and computational support by the Extreme Science and Engineering Discovery Environment (XSEDE) through allocation TG-OCE17001. A.M.P.M acknowledges support from NSF Award No. 1654663. T.W. was supported by NSF award OCE-1635414. RK acknowledges support via the Heisenberg program of the German Science Foundation under project number 469175784, the EU project TRIATLAS (European Union's Horizon 2020 programme, grant agreement No 817578) and a "Make Our Planet Great Again" grant of the ANR within the "Programme d'Investissements d'Avenir"; reference "ANR-19-MPGA-0012". Data generated by this analysis has been uploaded to BCO-DMO, DOI:10.26008/1912/bco-dmo.856942.1.

References

Alldredge, A. (1998). The carbon, nitrogen and mass content of marine snow as a function of aggregate size. *Deep-Sea Research Part I: Oceanographic Research Papers*, *45*(4-5), 529–541. doi: 10.1016/S0967-0637(97)00048-4

Alldredge, A. L., & Gotschalk, C. (1988). In situ settling behavior of marine snow. *Limnology and Oceanography*, *33*(3), 339–351. doi: 10.4319/lo.1988.33.3.0339

Alonso-González, I. J., Arístegui, J., Lee, C., Sanchez-Vidal, A., Calafat, A., Fabrés, J., ... Benítez-Barrios, V. (2010). Role of slowly settling particles in the ocean carbon cycle. *Geophysical Research Letters*, *37*(13). Retrieved from `https://agupubs.onlinelibrary.wiley.com/doi/abs/10.1029/2010GL043827` doi: https://doi.org/10.1029/2010GL043827

Arteaga, L., Haëntjens, N., Boss, E., Johnson, K. S., & Sarmiento, J. L. (2018). Assessment of Export Efficiency Equations in the Southern Ocean Applied to Satellite-Based Net Primary Production. *Journal of Geophysical Research: Oceans*, *123*(4), 2945–2964. doi: 10.1002/2018JC013787

Bianchi, D., Stock, C., Galbraith, E. D., & Sarmiento, J. L. (2013). Diel vertical migration: Ecological controls and impacts on the biological pump in a one-dimensional ocean model. *Global Biogeochemical Cycles*, *27*(2), 478–491. Retrieved from `https://agupubs.onlinelibrary.wiley.com/doi/abs/10.1002/gbc.20031` doi: https://doi.org/10.1002/gbc.20031

Bianchi, D., Weber, T. S., Kiko, R., & Deutsch, C. (2018). Global niche of marine anaerobic metabolisms expanded by particle microenvironments. *Nature Geoscience*, 1–6. Retrieved from `http://dx.doi.org/10.1038/s41561-018-0081-0` doi: 10.1038/s41561-018-0081-0

Bisson, K. M., Siegel, D. A., DeVries, T., Cael, B. B., & Buesseler, K. O. (2018). How Data Set Characteristics Influence Ocean Carbon Export Models. *Global Biogeochemical Cycles*, *32*(9), 1312–1328. doi: 10.1029/2018GB005934

Bourne, H. L., Bishop, J. K., Wood, T. J., Loew, T. J., & Liu, Y. (2019). Carbon Flux Explorer optical assessment of C, N and P fluxes. *Biogeosciences*, *16*(6), 1249–1264. doi: 10.5194/bg-16-1249-2019

Boyd, P. W., Claustre, H., Levy, M., Siegel, D. A., & Weber, T. (2019). Multi-faceted particle pumps drive carbon sequestration in the ocean. *Nature*, *568*(7752), 327–335. Retrieved from `https://doi.org/10.1038/s41586-019-1098-2` doi: 10.1038/s41586-019-1098-2

Buesseler, K., Antia, A., Chen, M., Fowler, S., Gardner, W., Gustafsson, O., ... Trull, T. (2007, 05). An assessment of the use of sediment traps for estimating upper ocean particle fuxes. *Journal of Marine Research*, *65*. doi: 10.1357/002224007781567621

Buesseler, K. O., & Boyd, P. W. (2009). Shedding light on processes that control particle export and flux attenuation in the twilight zone of the open ocean. *Limnology and Oceanography*, *54*(4), 1210–1232. doi: 10.4319/lo.2009.54.4.1210

Buesseler, K. O., Boyd, P. W., Black, E. E., & Siegel, D. A. (2020). Metrics that matter for assessing the ocean biological carbon pump. *Proceedings of the National Academy of Sciences of the United States of America*, *117*(18), 9679–9687. doi: 10.1073/pnas.1918114117

Cael, B., Cavan, E. L., & Britten, G. L. (2021). Reconciling the size-dependence of marine particle sinking speed. *Geophysical Research Letters*, *48*(5), e2020GL091771.

Carlson, C. A., Ducklow, H. W., & Michaels, A. F. (1994). Annual flux of dissolved organic carbon from the euphotic zone in the northwestern sargasso sea. *Nature*, *371*(6496), 405–408.

Clements, D. J., Yang, S., Weber, T., McDonnell, A. M. P., Kiko, R., Stemmann, L., & Bianchi, D. (2022). Constraining the Particle Size Distribution of Large Marine Particles in the Global Ocean With In Situ Optical Observations and

Supervised Learning. *Global Biogeochemical Cycles*, *36*(5), e2021GB007276. Retrieved from https://agupubs.onlinelibrary.wiley.com/doi/abs/10.1029/2021GB007276 doi: https://doi.org/10.1029/2021GB007276

Cram, J. A., Weber, T., Leung, S. W., McDonnell, A. M., Liang, J. H., & Deutsch, C. (2018). The Role of Particle Size, Ballast, Temperature, and Oxygen in the Sinking Flux to the Deep Sea. *Global Biogeochemical Cycles*, *32*(5), 858–876. doi: 10.1029/2017GB005710

Dall'Olmo, G., Dingle, J., Polimene, L., Brewin, R. J., & Claustre, H. (2016). Substantial energy input to the mesopelagic ecosystem from the seasonal mixed-layer pump. *Nature Geoscience*, *9*(11), 820–823. doi: 10.1038/ngeo2818

DeVries, T., Holzer, M., & Primeau, F. (2017). Recent increase in oceanic carbon uptake driven by weaker upper-ocean overturning. *Nature*, *542*(7640), 215–218. Retrieved from http://dx.doi.org/10.1038/nature21068 doi: 10.1038/nature21068

DeVries, T., Primeau, F., & Deutsch, C. (2012). The sequestration efficiency of the biological pump. *Geophysical Research Letters*, *39*(13).

DeVries, T., & Weber, T. (2017). The export and fate of organic matter in the ocean: New constraints from combining satellite and oceanographic tracer observations. *Global Biogeochemical Cycles*, *31*(3), 535–555. doi: 10.1002/2016GB005551

Dunne, J. P., Sarmiento, J. L., & Gnanadesikan, A. (2007). A synthesis of global particle export from the surface ocean and cycling through the ocean interior and on the seafloor. *Global Biogeochemical Cycles*, *21*(4), 1–16. doi: 10.1029/2006GB002907

Durkin, C. A., Estapa, M. L., & Buesseler, K. O. (2015). Observations of carbon export by small sinking particles in the upper mesopelagic. *Marine Chemistry*, *175*, 72–81. Retrieved from https://www.sciencedirect.com/science/article/pii/S0304420315000390 doi: https://doi.org/10.1016/j.marchem.2015.02.011

Emerson. (2013). Global Biogeochemical Cycles the biological carbon flux in the ocean. *Global Biogeochemical Cycles*, 14–28. doi: 10.1002/2013GB004680

Fontanez, K. M., Eppley, J. M., Samo, T. J., Karl, D. M., & DeLong, E. F. (2015). Microbial community structure and function on sinking particles in the north pacific subtropical gyre. *Frontiers in microbiology*, *6*, 469.

Forest, A., Stemmann, L., Picheral, M., Burdorf, L., Robert, D., Fortier, L., & Babin, M. (2012). Size distribution of particles and zooplankton across the shelf-basin system in southeast Beaufort Sea: Combined results from an Underwater Vision Profiler and vertical net tows. *Biogeosciences*, *9*(4), 1301–1320. doi: 10.5194/bg-9-1301-2012

Gaiero, D., Probst, J.-L., Depetris, P., Bidart, S., & Leleyter, L. (2003). Iron and other transition metals in patagonian riverborne and windborne materials: geochemical control and transport to the southern south atlantic ocean. *Geochimica et Cosmochimica Acta*, *67*(19), 3603-3623. Retrieved from https://www.sciencedirect.com/science/article/pii/S0016703703002114 doi: https://doi.org/10.1016/S0016-7037(03)00211-4

Guidi, L., Chaffron, S., Bittner, L., Eveillard, D., Larhlimi, A., Roux, S., ... Gorsky, G. (2016). Plankton networks driving carbon export in the oligotrophic ocean. *Nature*, *532*(7600), 465–470. Retrieved from http://dx.doi.org/10.1038/nature16942 doi: 10.1038/nature16942

Guidi, L., Jackson, G. A., Stemmann, L., Miquel, J. C., Picheral, M., & Gorsky, G. (2008). Relationship between particle size distribution and flux in the mesopelagic zone. *Deep-Sea Research Part I: Oceanographic Research Papers*, *55*(10), 1364–1374. doi: 10.1016/j.dsr.2008.05.014

Guidi, L., Legendre, L., Reygondeau, G., Uitz, J., Stemmann, L., & Henson, S. A. (2015, jul). A new look at ocean carbon remineralization for estimating

deepwater sequestration. *Global Biogeochemical Cycles*, *29*(7), 1044–1059. Retrieved from http://doi.wiley.com/10.1002/2014GB005063 doi: 10.1002/2014GB005063

Guidi, L., Stemmann, L., Jackson, G. A., Ibanez, F., Claustre, H., Legendre, L., ... Gorsky, G. (2009). Effects of phytoplankton community on production, size and export of large aggregates: A world-ocean analysis. *Limnology and Oceanography*, *54*(6), 1951–1963. doi: 10.4319/lo.2009.54.6.1951

Henson, S. A., Sanders, R., Madsen, E., Morris, P. J., Le Moigne, F., & Quartly, G. D. (2011). A reduced estimate of the strength of the ocean's biological carbon pump. *Geophysical Research Letters*, *38*(4), 10–14. doi: 10.1029/2011GL046735

Honjo, S., Manganini, S. J., Krishfield, R. A., & Francois, R. (2008). Particulate organic carbon fluxes to the ocean interior and factors controlling the biological pump: A synthesis of global sediment trap programs since 1983. *Progress in Oceanography*, *76*(3), 217-285. Retrieved from https://www.sciencedirect.com/science/article/pii/S0079661108000025 doi: https://doi.org/10.1016/j.pocean.2007.11.003

Johnson, G. C., Schmidtko, S., & Lyman, J. M. (2012). Relative contributions of temperature and salinity to seasonal mixed layer density changes and horizontal density gradients. *Journal of Geophysical Research: Oceans*, *117*(4). doi: 10.1029/2011JC007651

Jouandet, M. P., Jackson, G. A., Carlotti, F., Picheral, M., Stemmann, L., & Blain, S. (2014). Rapid formation of large aggregates during the spring bloom of Kerguelen Island: Observations and model comparisons. *Biogeosciences*, *11*(16), 4393–4406. doi: 10.5194/bg-11-4393-2014

Karl, D., Knauer, G., Martin, J., & Ward, B. (1984). Bacterial chemolithotrophy in the ocean is associated with sinking particles. *Nature*, *309*(5963), 54–56.

Kiko, R., Biastoch, A., Brandt, P., Cravatte, S., Hauss, H., Hummels, R., ... Stemmann, L. (2017). Biological and physical influences on marine snowfall at the equator. *Nature Geoscience*, *10*(11), 852–858. doi: 10.1038/NGEO3042

Kiko, R., Picheral, M., Antoine, D., Babin, M., Berline, L., Biard, T., ... Stemmann, L. (2022). A global marine particle size distribution dataset obtained with the Underwater Vision Profiler 5. *Earth System Science Data*, *14*(9), 4315–4337. Retrieved from https://essd.copernicus.org/articles/14/4315/2022/ doi: 10.5194/essd-14-4315-2022

Kriest, I. (2002). Different parameterizations of marine snow in a 1D-model and their influence on representation of marine snow, nitrogen budget and sedimentation. *Deep-Sea Research Part I: Oceanographic Research Papers*, *49*(12), 2133–2162. doi: 10.1016/S0967-0637(02)00127-9

Kwon, E. Y., Primeau, F., & Sarmiento, J. L. (2009). The impact of remineralization depth on the air–sea carbon balance. *Nature Geoscience*, *2*(9), 630–635.

Laws, E. A., D'Sa, E., & Naik, P. (2011). Simple equations to estimate ratios of new or export production to total production from satellite-derived estimates of sea surface temperature and primary production. *Limnology and Oceanography: Methods*, *9*(DECEMBER), 593–601. doi: 10.4319/lom.2011.9.593

Le Gland, G., Aumont, O., & Mémery, L. (2019). An estimate of thorium 234 partition coefficients through global inverse modeling. *Journal of Geophysical Research: Oceans*, *124*(6), 3575-3606. Retrieved from https://agupubs.onlinelibrary.wiley.com/doi/abs/10.1029/2018JC014668 doi: https://doi.org/10.1029/2018JC014668

Longhurst, A., Bedo, A., Harrison, W., Head, E., & Sameoto, D. (1990). Vertical flux of respiratory carbon by oceanic diel migrant biota. *Deep Sea Research Part A. Oceanographic Research Papers*, *37*(4), 685–694.

Martin, J. H., Knauer, G. A., Karl, D. M., & Broenkow, W. W. (1987). VERTEX: carbon cycling in the northeast Pacific. *Deep Sea Research Part A, Oceano-*

graphic Research Papers, *34*(2), 267–285. doi: 10.1016/0198-0149(87)90086-0

Morel, A., Huot, Y., Gentili, B., Werdell, P. J., Hooker, S. B., & Franz, B. A. (2007). Examining the consistency of products derived from various ocean color sensors in open ocean (Case 1) waters in the perspective of a multi-sensor approach. *Remote Sensing of Environment*, *111*(1), 69–88. doi: 10.1016/j.rse.2007.03.012

Mouw, C. B., Barnett, A., McKinley, G. A., Gloege, L., & Pilcher, D. (2016). Global ocean particulate organic carbon flux merged with satellite parameters. *Earth System Science Data*, *8*(2), 531–541.

Nishioka, J., Obata, H., Ogawa, H., Ono, K., Yamashita, Y., Lee, K., ... Yasuda, I. (2020). Subpolar marginal seas fuel the North Pacific through the intermediate water at the termination of the global ocean circulation. *Proceedings of the National Academy of Sciences of the United States of America*, *117*(23), 12665–12673. doi: 10.1073/pnas.2000658117

Omand, M. M., D'Asaro, E. A., Lee, C. M., Perry, M. J., Briggs, N., Cetinić, I., & Mahadevan, A. (2015). Eddy-driven subduction exports particulate organic carbon from the spring bloom. *Science*, *348*(6231), 222–225. doi: 10.1126/science.1260062

Palevsky, H. I., & Doney, S. C. (2018). How Choice of Depth Horizon Influences the Estimated Spatial Patterns and Global Magnitude of Ocean Carbon Export Flux. *Geophysical Research Letters*, *45*(9), 4171–4179. doi: 10.1029/2017GL076498

Pavia, F. J., Anderson, R. F., Lam, P. J., Cael, B. B., Vivancos, S. M., Fleisher, M. Q., ... Edwards, R. L. (2019). Shallow particulate organic carbon regeneration in the South Pacific Ocean. *Proceedings of the National Academy of Sciences*, *116*(20), 201901863. doi: 10.1073/pnas.1901863116

Picheral, M., Catalano, C., Brousseau, D., Claustre, H., Coppola, L., Leymarie, E., ... others (2022). The underwater vision profiler 6: an imaging sensor of particle size spectra and plankton, for autonomous and cabled platforms. *Limnology and Oceanography: Methods*, *20*(2), 115–129.

Picheral, M., Guidi, L., Stemmann, L., Karl, D. M., Iddaoud, G., & Gorsky, G. (2010). The underwater vision profiler 5: An advanced instrument for high spatial resolution studies of particle size spectra and zooplankton. *Limnology and Oceanography: Methods*, *8*(SEPT), 462–473. doi: 10.4319/lom.2010.8.462

Quay, P., Emerson, S., & Palevsky, H. (2020). Regional Pattern of the Ocean's Biological Pump Based on Geochemical Observations. *Geophysical Research Letters*, *47*(14), 1–10. doi: 10.1029/2020GL088098

Reynolds, R., Stramski, D., Wright, V., & Woźniak, S. (2010). Measurements and characterization of particle size distributions in coastal waters. *Journal of Geophysical Research: Oceans*, *115*(C8).

Reynolds, R. A., & Stramski, D. (2021). Variability in oceanic particle size distributions and estimation of size class contributions using a non-parametric approach. *Journal of Geophysical Research: Oceans*, *126*(12), e2021JC017946.

Richardson, T. L. (2019). Mechanisms and pathways of small-phytoplankton export from the surface ocean. *Ann. Rev. Mar. Sci*, *11*(1), 57–74.

Riley, J. S., Sanders, R., Marsay, C., Le Moigne, F. A., Achterberg, E. P., & Poulton, A. J. (2012). The relative contribution of fast and slow sinking particles to ocean carbon export. *Global Biogeochemical Cycles*, *26*(1), 1–10. doi: 10.1029/2011GB004085

Robinson, C., Steinberg, D. K., Anderson, T. R., Aristegui, J., Carlson, C. A., Frost, J. R., ... others (2010). Mesopelagic zone ecology and biogeochemistry–a synthesis. *Deep Sea Research Part II: Topical Studies in Oceanography*, *57*(16), 1504–1518.

Séférian, R., Berthet, S., Yool, A., Palmieri, J., Bopp, L., Tagliabue, A., ... others (2020). Tracking improvement in simulated marine biogeochemistry between

cmip5 and cmip6. *Current Climate Change Reports*, 1–25.

Siegel, D. A., Buesseler, K. O., Doney, S. C., Sailley, S. F., Behrenfeld, M. J., & Boyd, P. W. (2014). Global assessment of ocean carbon export by combining satellite observations and food-web models. *Global Biogeochemical Cycles*, *28*(3), 181–196. doi: 10.1002/2013GB004743

Siegel, D. A., DeVries, T., Cetinić, I., & Bisson, K. M. (2022). Quantifying the ocean's biological pump and its carbon cycle impacts on global scales. *Annual Review of Marine Science*, *15*.

Smayda, T. J. (1970). The Suspension and sinking of phytoplankton in the sea. *Oceanography Marine Biology, Annual Review*(8), 353–414.

Steinberg, D. K., Carlson, C. A., Bates, N. R., Goldthwait, S. A., Madin, L. P., & Michaels, A. F. (2000). Zooplankton vertical migration and the active transport of dissolved organic and inorganic carbon in the sargasso sea. *Deep Sea Research Part I: Oceanographic Research Papers*, *47*(1), 137–158.

Stemmann, L., & Boss, E. (2012). Plankton and Particle Size and Packaging: From Determining Optical Properties to Driving the Biological Pump. *Annual Review of Marine Science*, *4*(1), 263–290. Retrieved from `http://www.annualreviews.org/doi/10.1146/annurev-marine-120710-100853` doi: 10.1146/annurev-marine-120710-100853

Stemmann, L., Eloire, D., Sciandra, A., Jackson, G., Guidi, L., Picheral, M., & Gorsky, G. (2008). Volume distribution for particles between 3.5 to 2000 μm in the upper 200 m region of the South Pacific Gyre. *Biogeosciences Discussions*, *5*, 299–310. doi: 10.5194/bgd-4-3377-2007

Stemmann, L., Jackson, G. A., & Ianson, D. (2004). A vertical model of particle size distributions and fluxes in the midwater column that includes biological and physical processes - Part I: Model formulation. *Deep-Sea Research Part I: Oceanographic Research Papers*, *51*(7), 865–884. doi: 10.1016/j.dsr.2004.03.001

Stemmann, L., Youngbluth, M., Robert, K., Hosia, A., Picheral, M., Paterson, H., ... Gorsky, G. (2008). Global zoogeography of fragile macrozooplankton in the upper 100-1000 m inferred from the underwater video profiler. *ICES Journal of Marine Science*, *65*(3), 433–442. doi: 10.1093/icesjms/fsn010

Stukel, M. R., Aluwihare, L. I., Barbeau, K. A., Chekalyuk, A. M., Goericke, R., Miller, A. J., ... Landry, M. R. (2017). Mesoscale ocean fronts enhance carbon export due to gravitational sinking and subduction. *Proceedings of the National Academy of Sciences*, *114*(6), 1252–1257. Retrieved from `http://www.pnas.org/lookup/doi/10.1073/pnas.1609435114` doi: 10.1073/pnas.1609435114

Trudnowska, E., Lacour, L., Ardyna, M., Rogge, A., Irisson, J. O., Waite, A. M., ... Stemmann, L. (2021). Marine snow morphology illuminates the evolution of phytoplankton blooms and determines their subsequent vertical export. *Nature communications*, *12*(1), 1–13.

Trudnowska, E., Stemmann, L., Błachowiak-Samołyk, K., & Kwasniewski, S. (2020). Taxonomic and size structures of zooplankton communities in the fjords along the atlantic water passage to the arctic. *Journal of Marine Systems*, *204*, 103306. Retrieved from `https://www.sciencedirect.com/science/article/pii/S0924796320300026` doi: https://doi.org/10.1016/j.jmarsys.2020.103306

Turner, J. T. (2015). Zooplankton fecal pellets, marine snow, phytodetritus and the ocean's biological pump. *Progress in Oceanography*, *130*, 205–248.

Volk, T., & Hoffert, M. I. (1985). Ocean carbon pumps: Analysis of relative strengths and efficiencies in ocean-driven atmospheric co2 changes. In *The carbon cycle and atmospheric co2: Natural variations archean to present* (p. 99-110). American Geophysical Union (AGU). Retrieved from `https://agupubs.onlinelibrary.wiley.com/doi/abs/10.1029/GM032p0099` doi: https://doi.org/10.1029/GM032p0099

Weber, T., Cram, J. A., Leung, S. W., DeVries, T., & Deutsch, C. (2016). Deep ocean nutrients imply large latitudinal variation in particle transfer efficiency. *Proceedings of the National Academy of Sciences of the United States of America*, *113*(31), 8606–8611. doi: 10.1073/pnas.1604414113

Figure 1.

a) Reconstructed PSD Biovolume

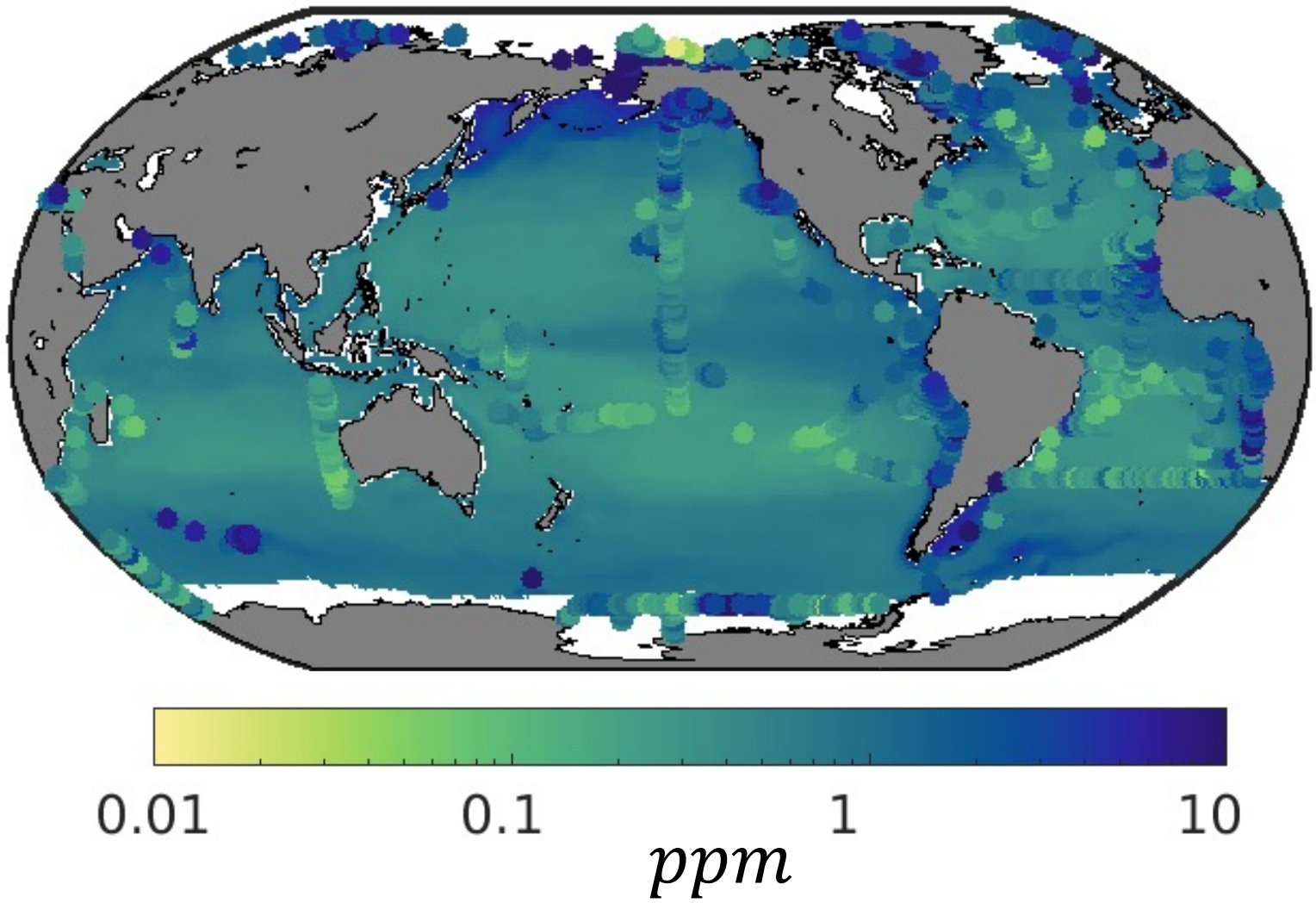

b) Reconstructed PSD Slope

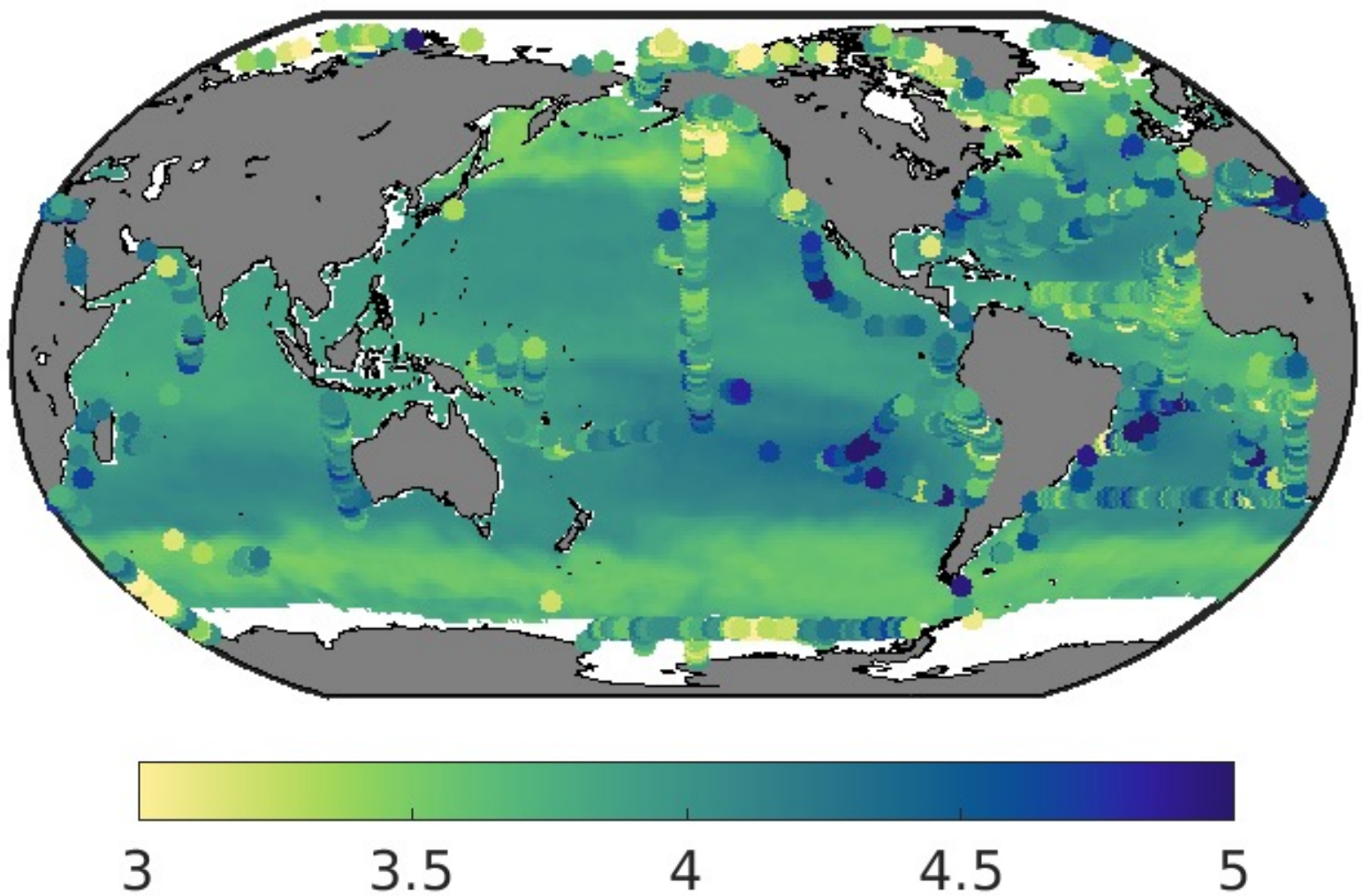

Figure 2.

a) This Study vs *in situ* data

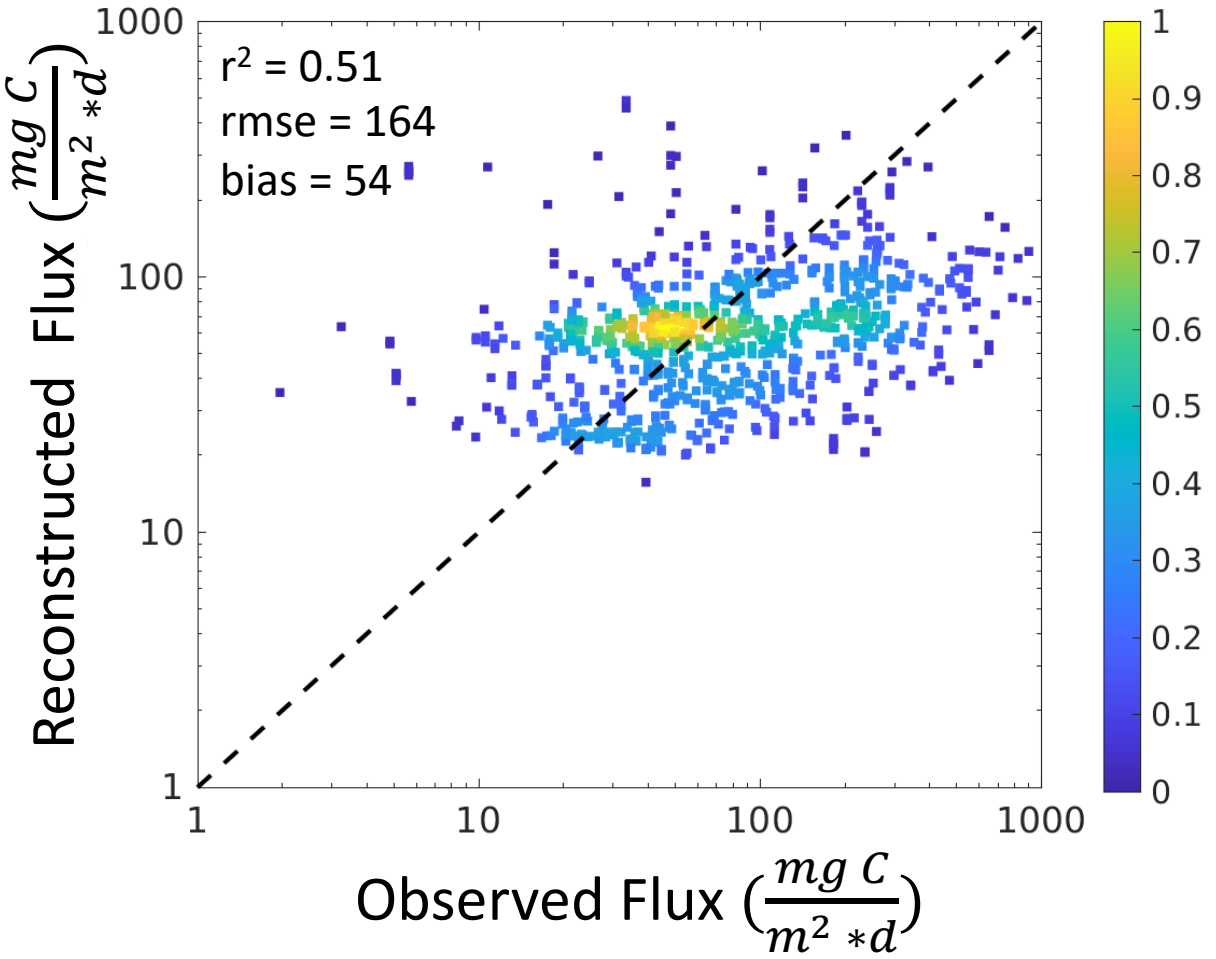

b) Siegel et al. (2014) vs *in situ* data

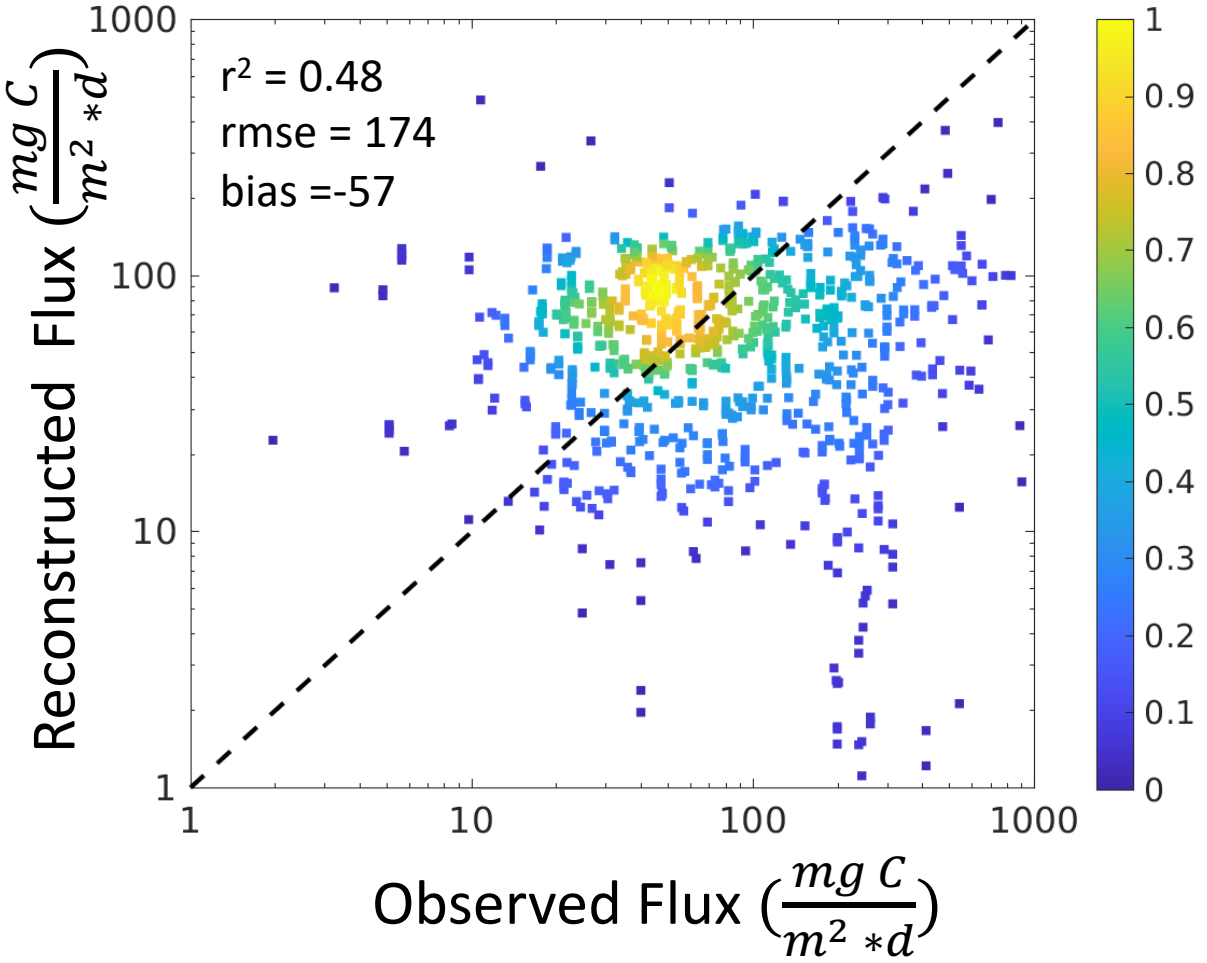

c) Henson et al. (2011) vs *in situ* data

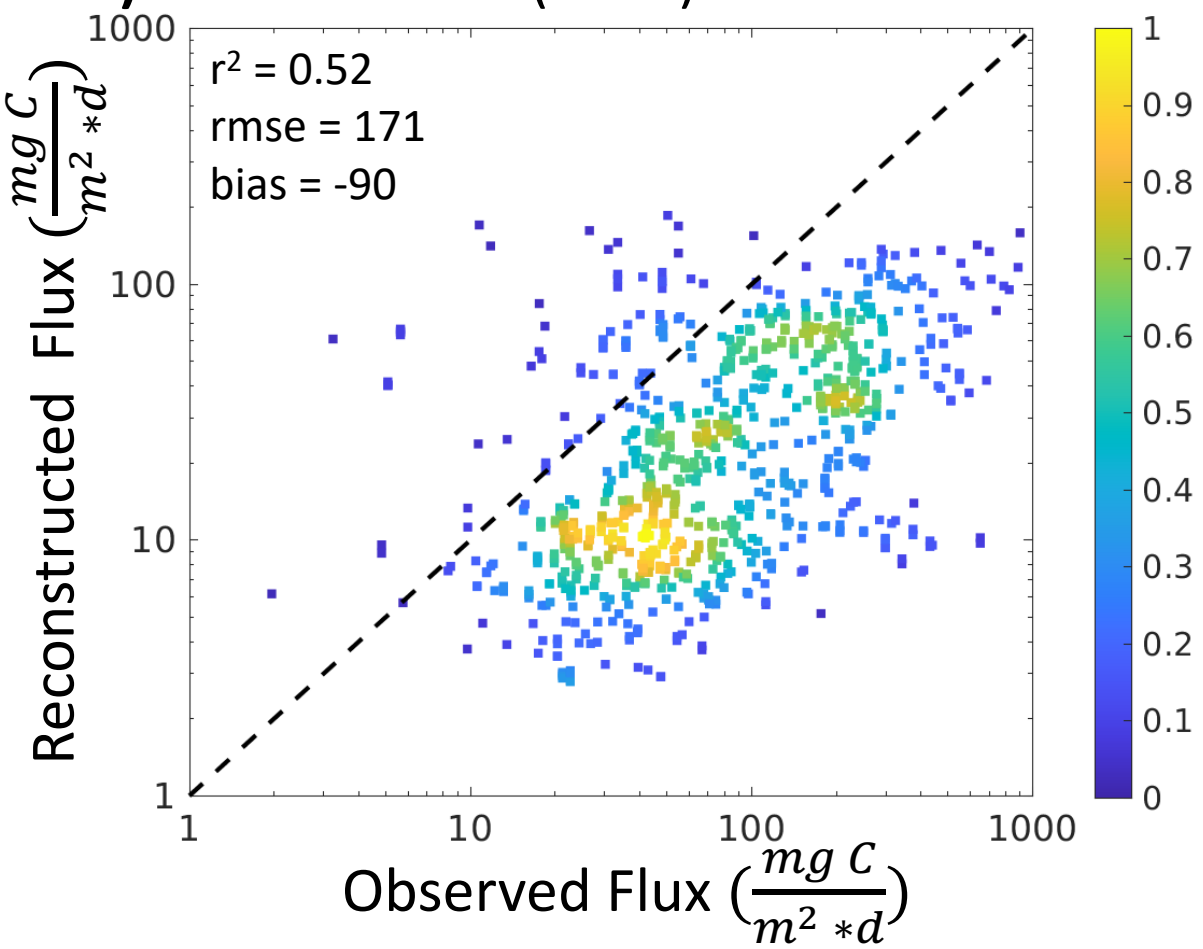

d) Dunne et al. (2007) vs *in situ* data

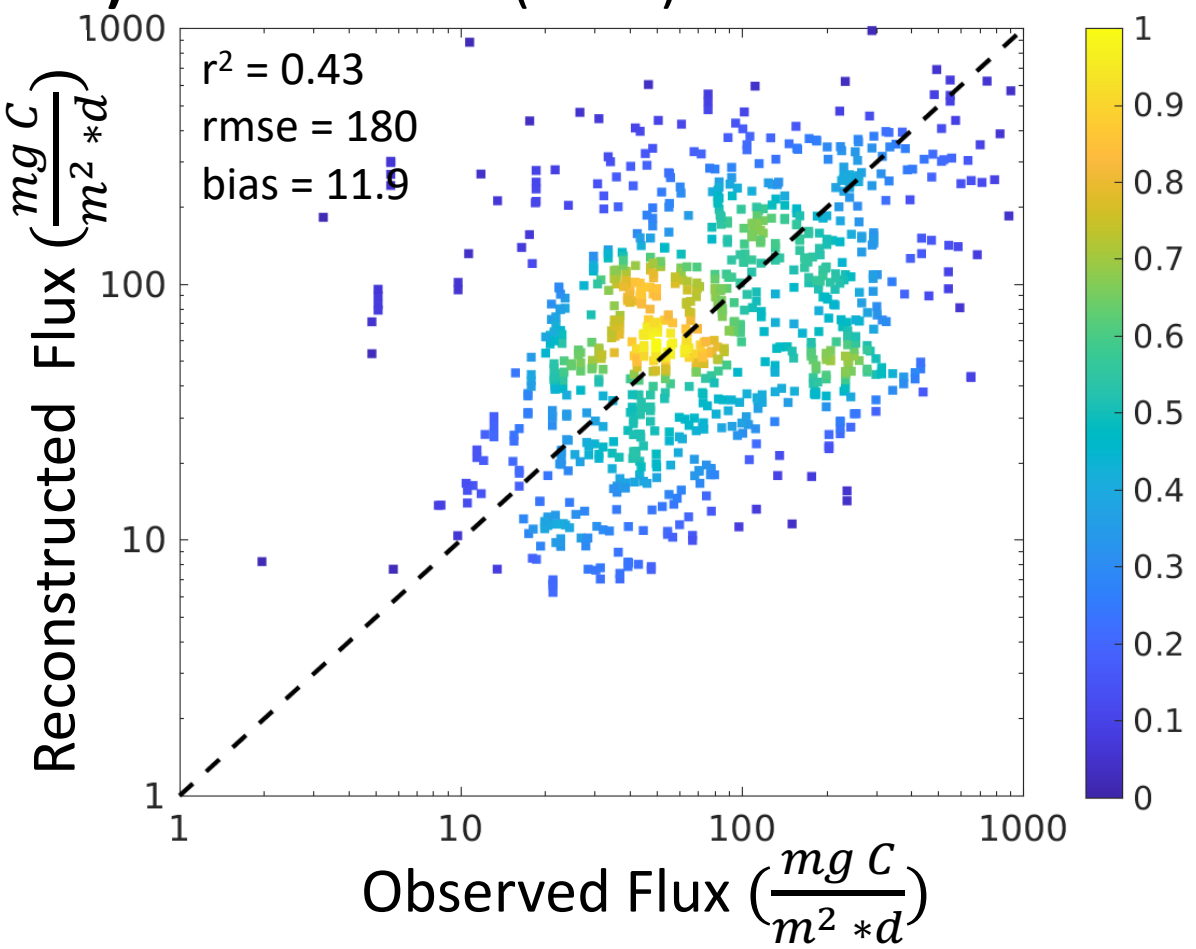

Figure 3.

a) This Study

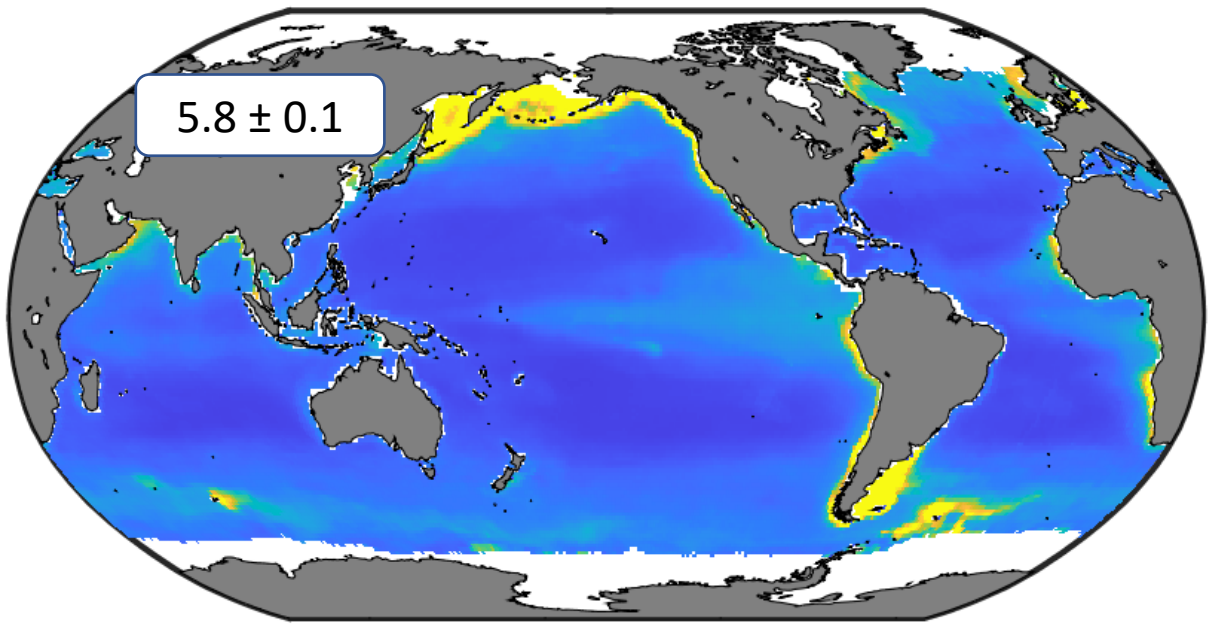

b) Bisson et al. (2018)

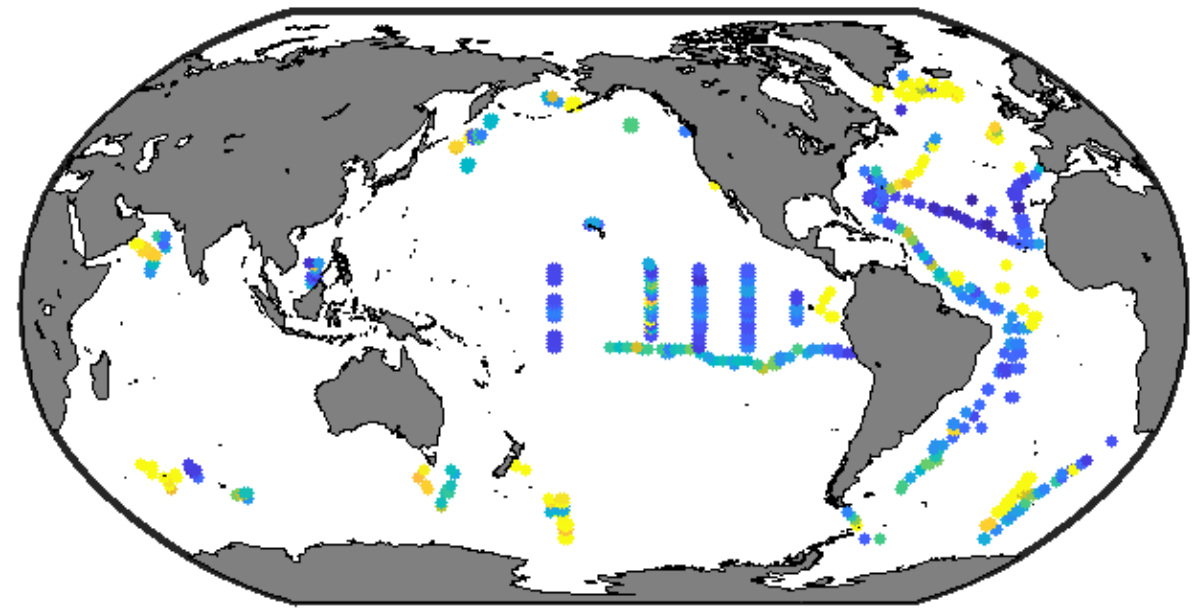

c) Devries and Weber (2017)

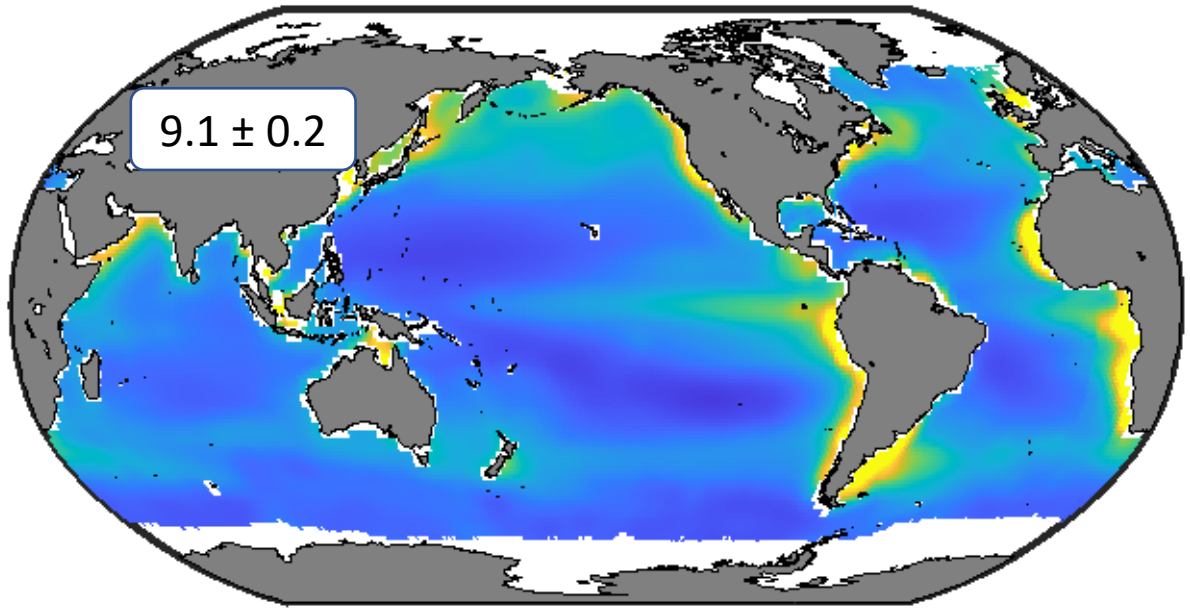

d) Dunne et al. (2007)

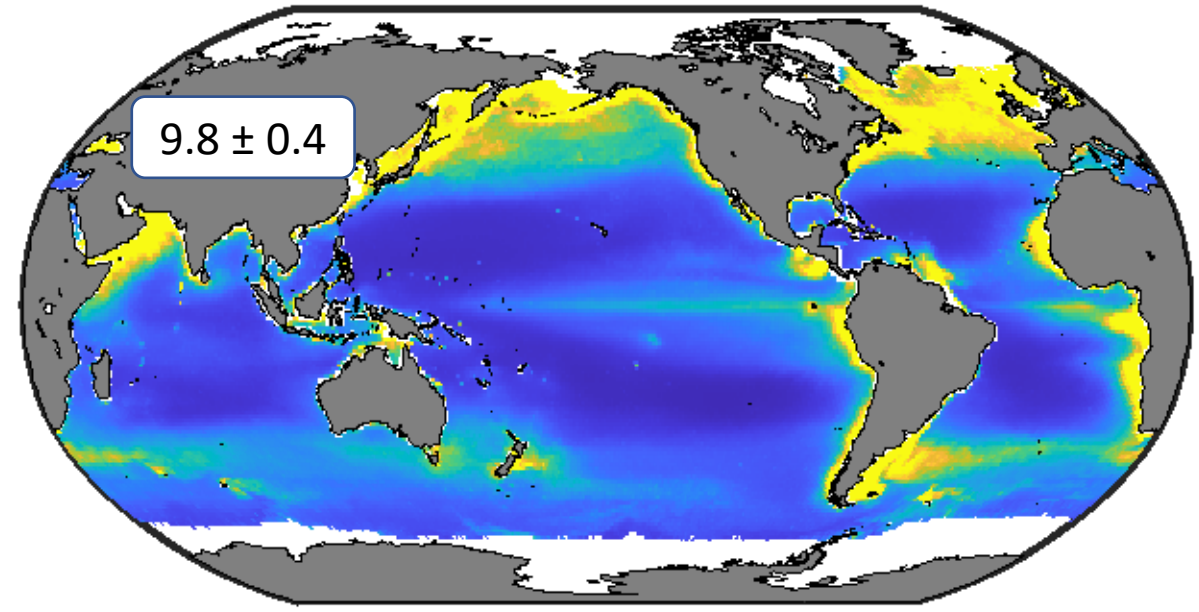

e) Siegel et al. (2014)

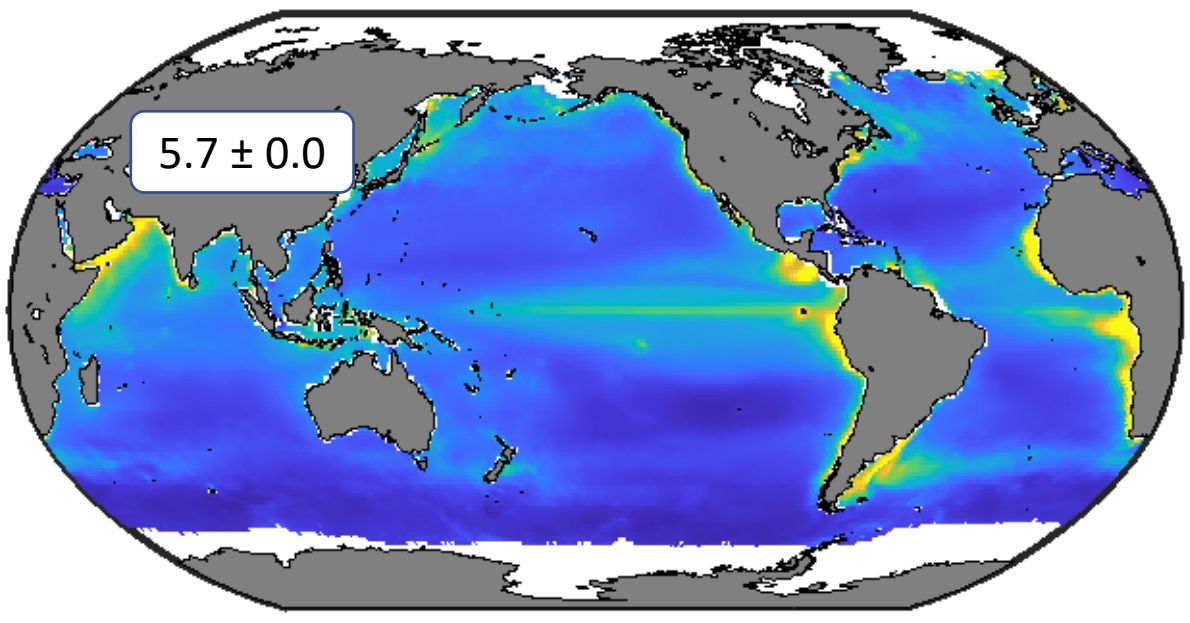

f) Henson et al. (2011)

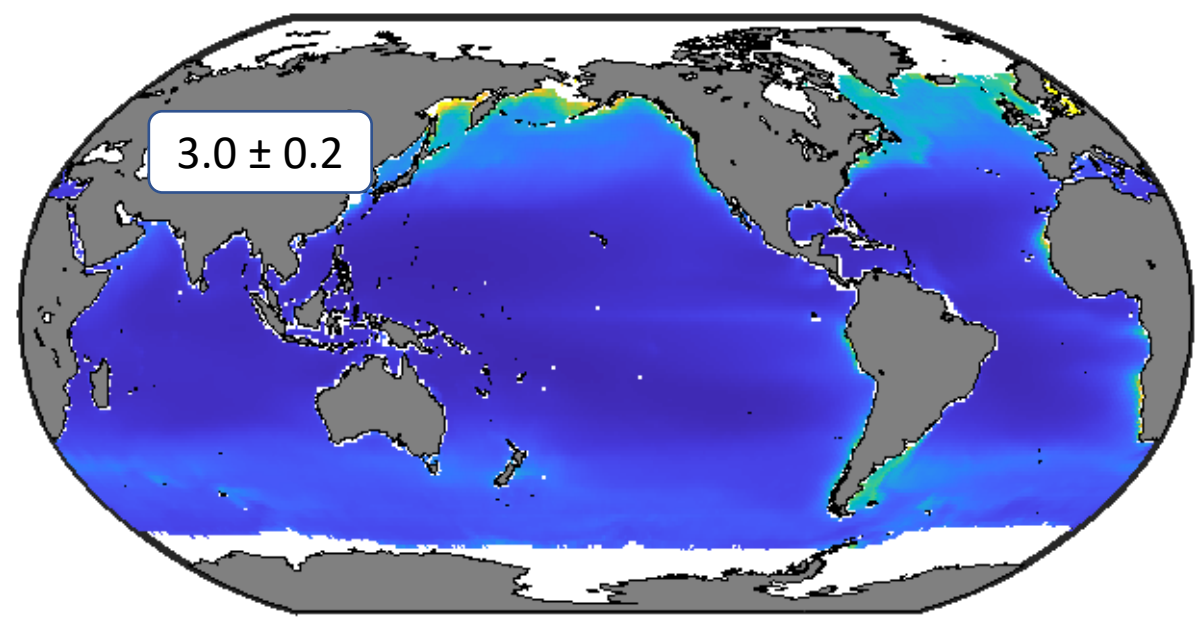

$mg\ C\ m^{-2} d^{-1}$

Figure 4.

a) Small Particle Fraction

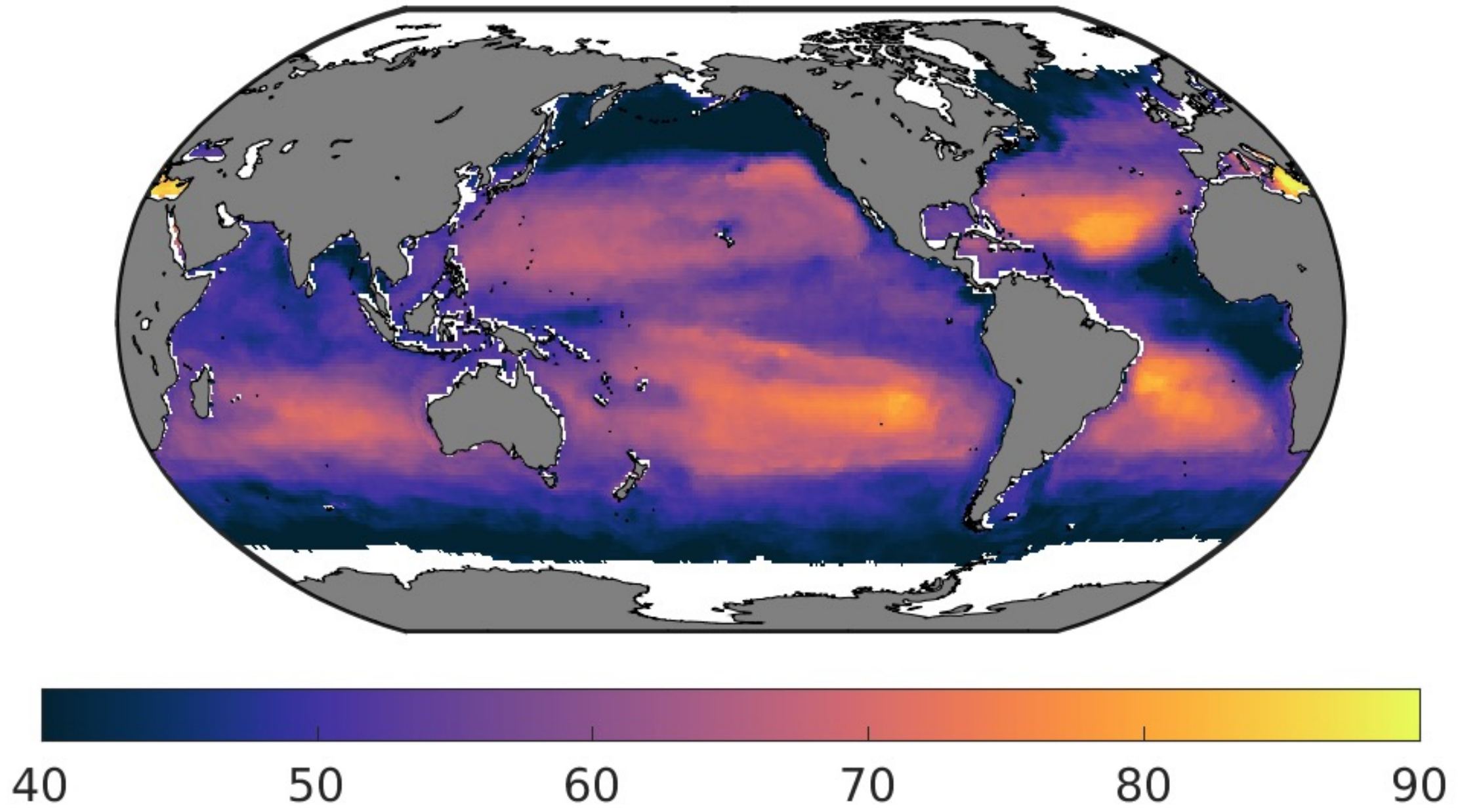

b) Large Particle Fraction

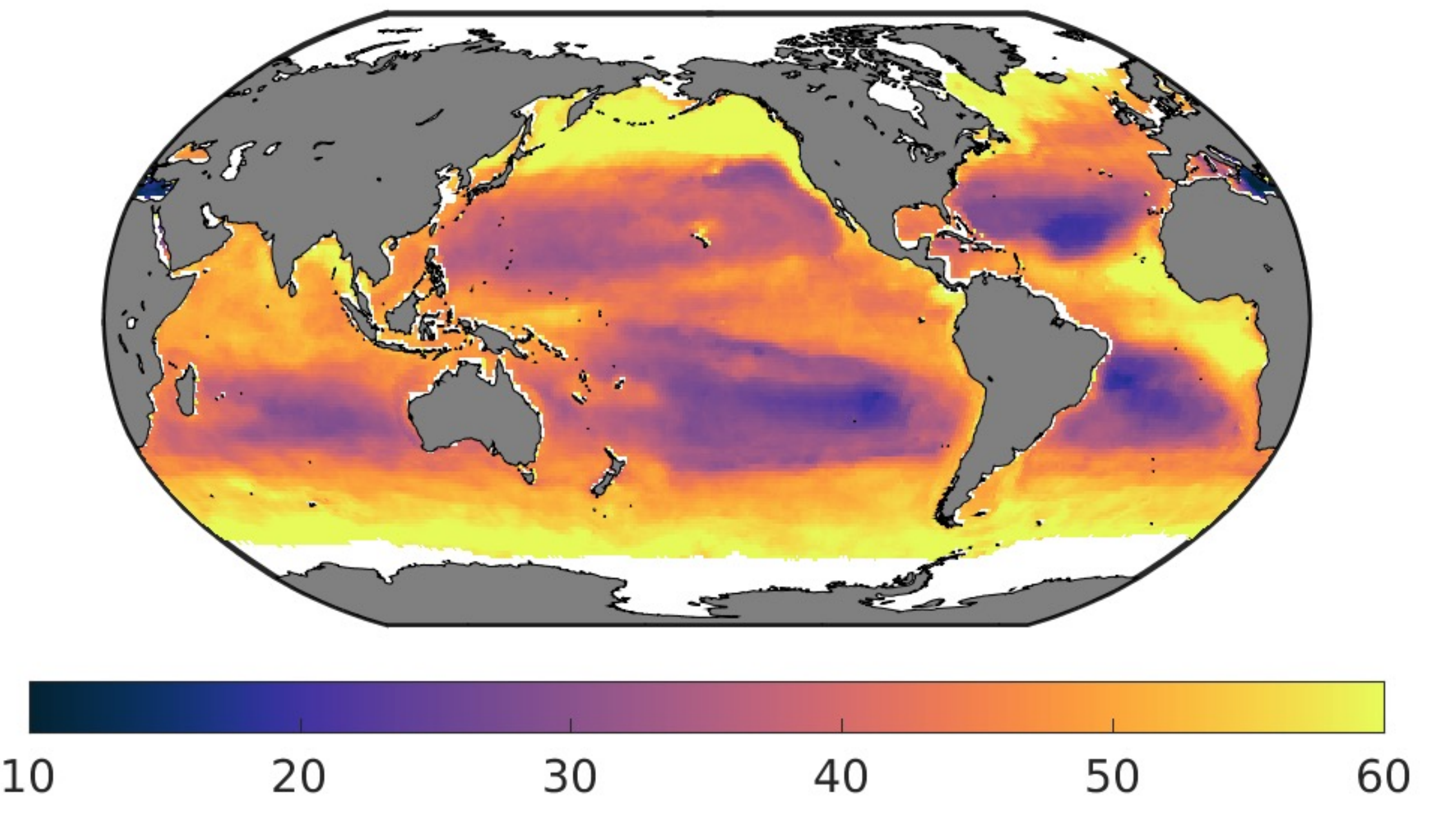

Figure 5.

a)

Global Ocean

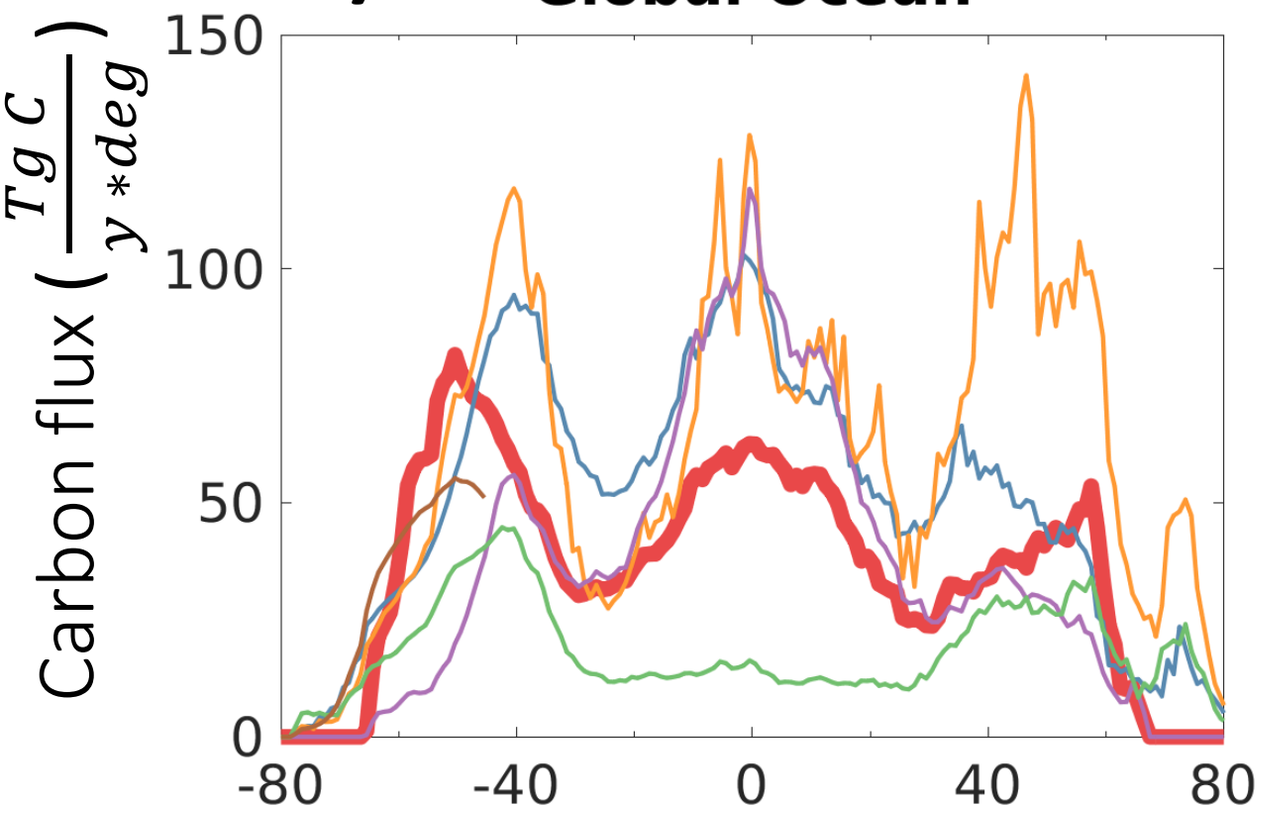

b)

Pacific Ocean

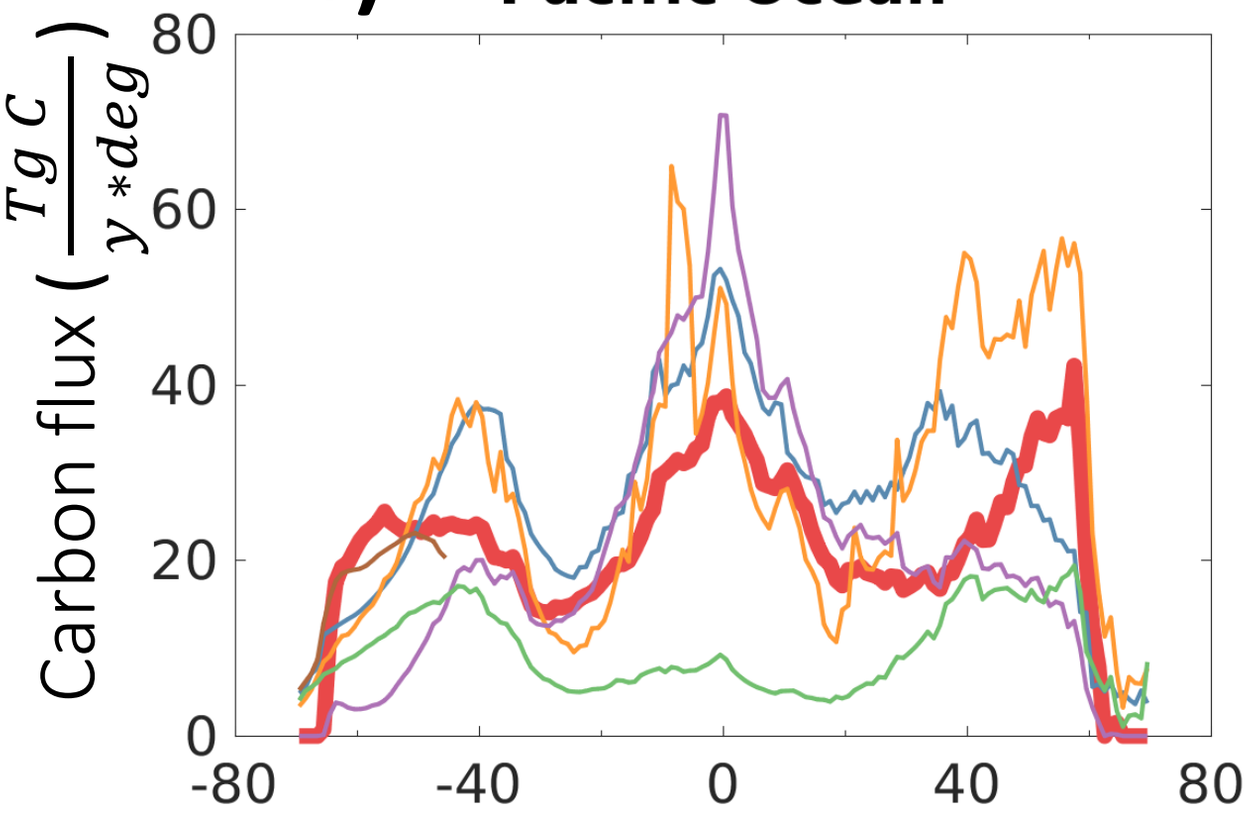

c)

Atlantic Ocean

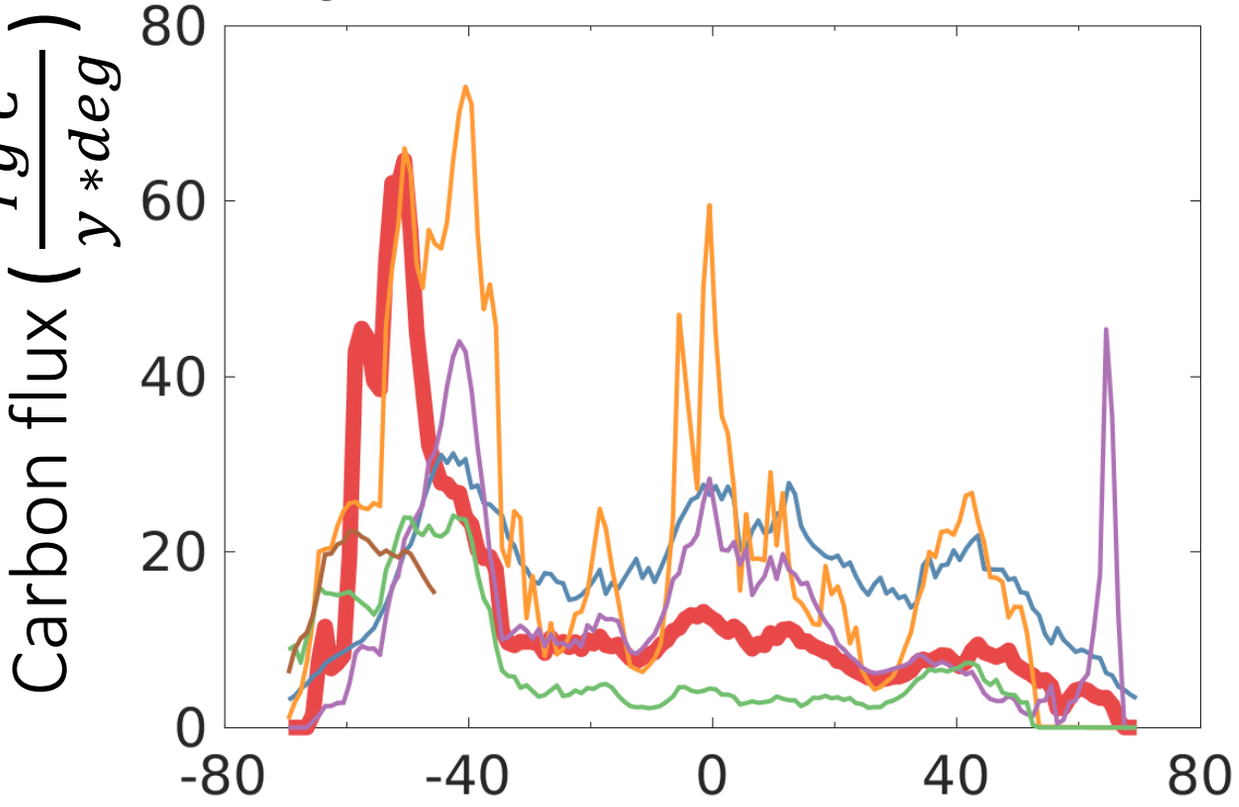

d)

Indian Ocean

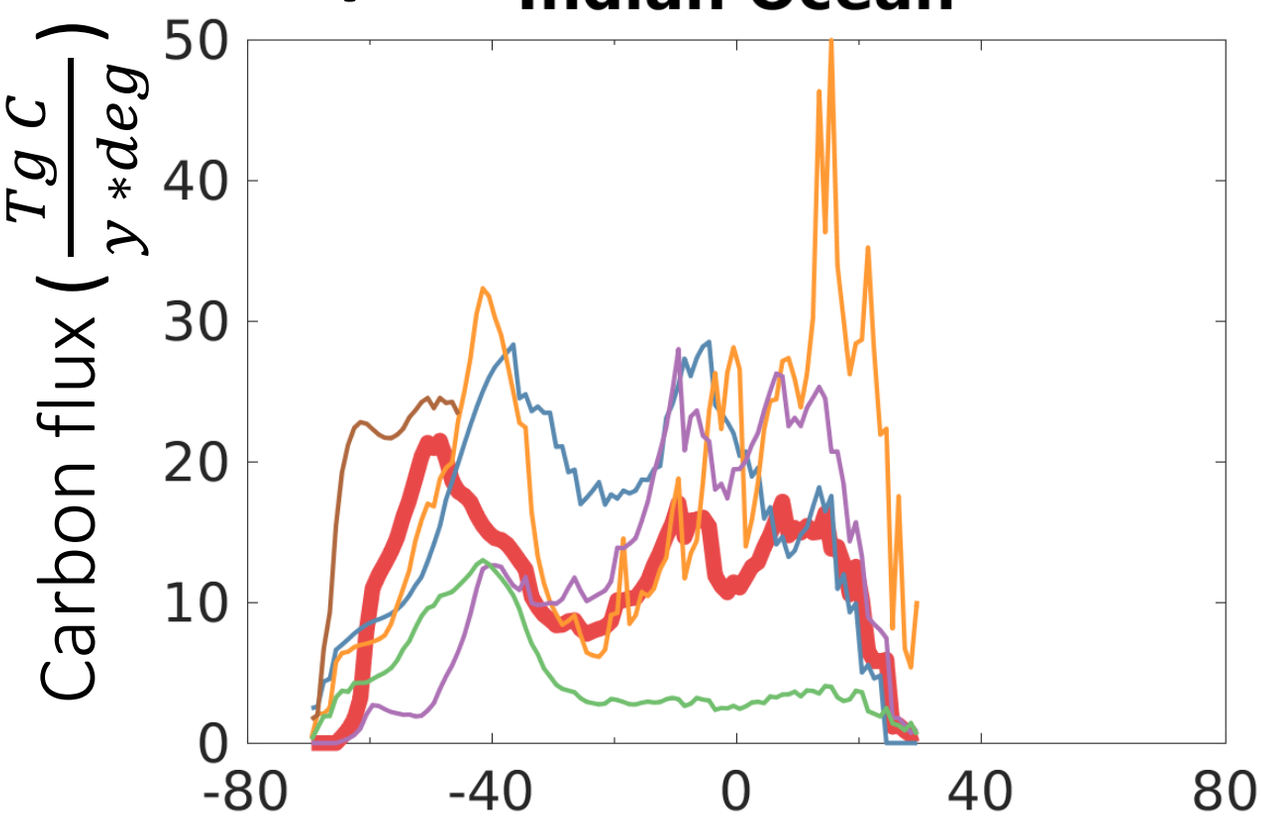

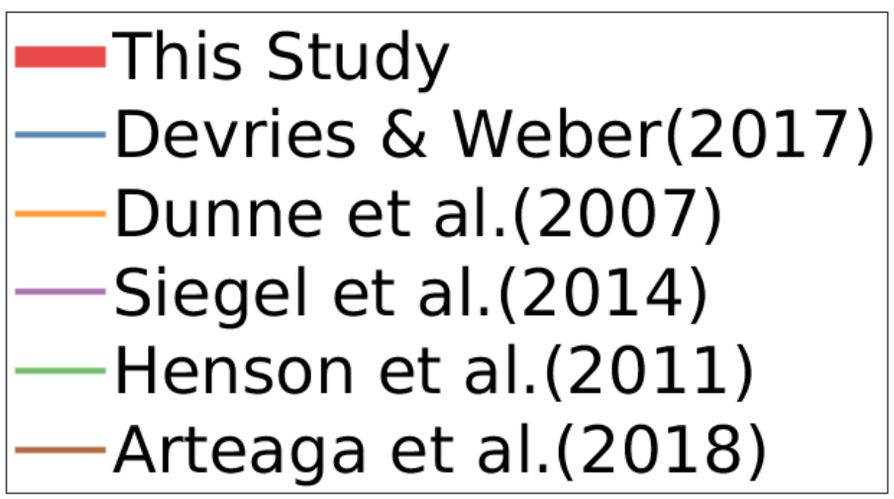

Figure 6.

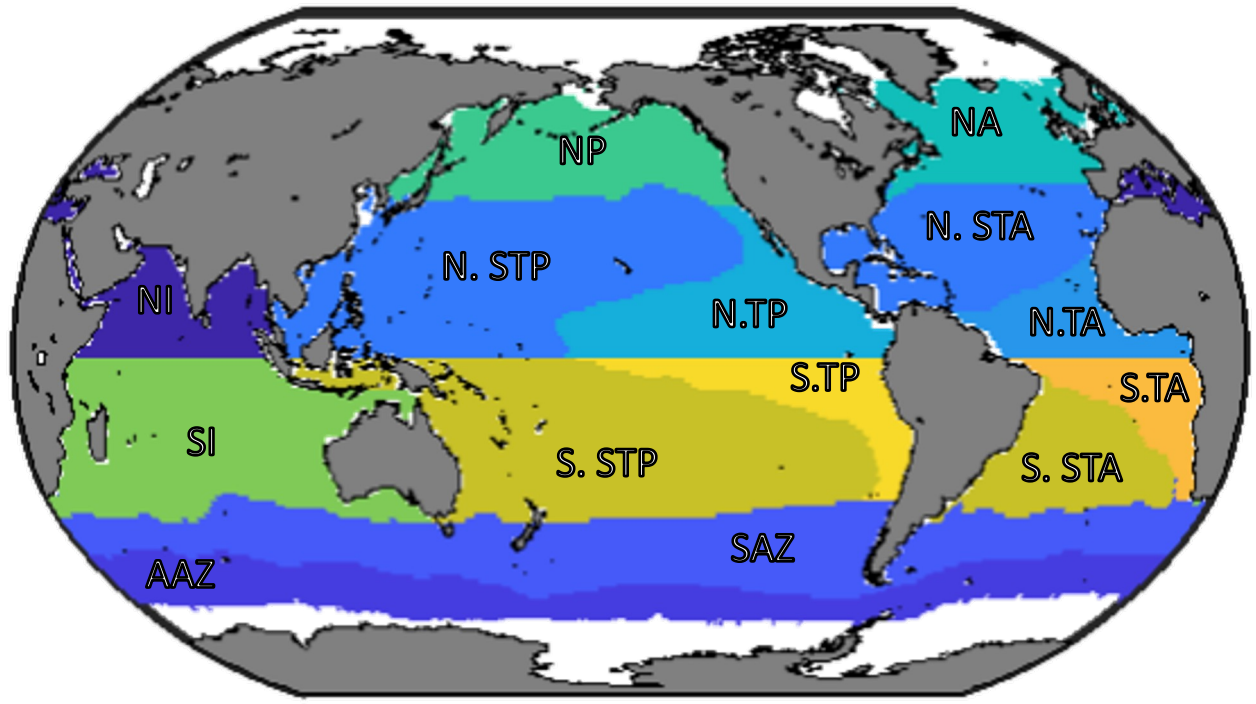

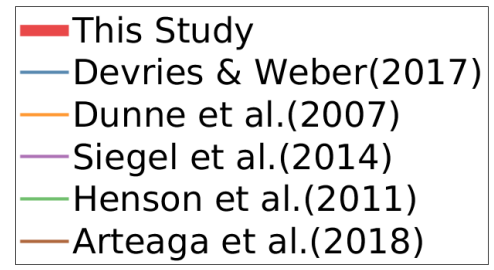

N. Pacific (NP)

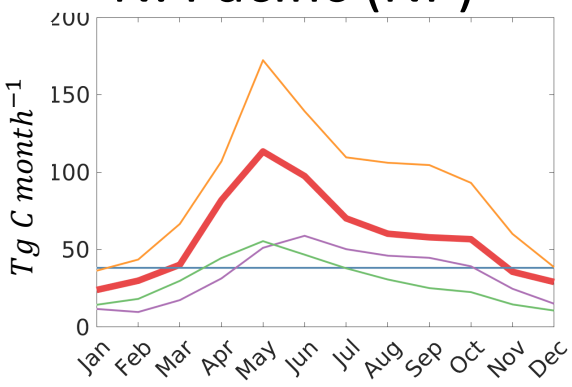

N. Atlantic (NA)

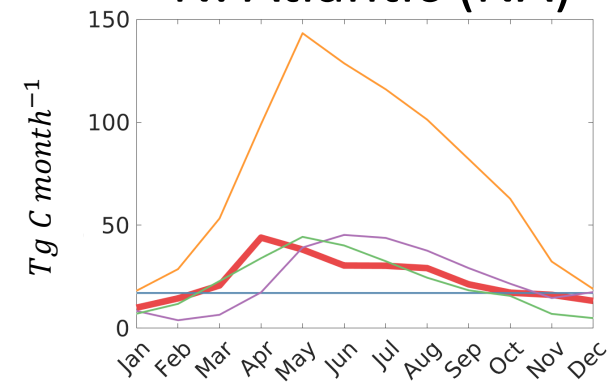

N. TA

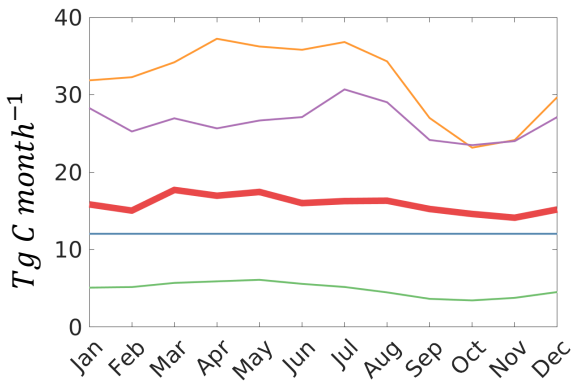

N. STP

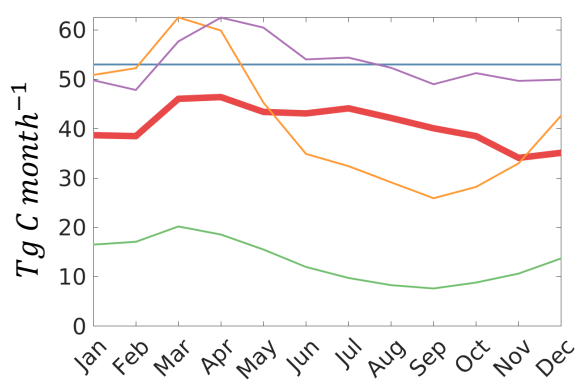

N. TP

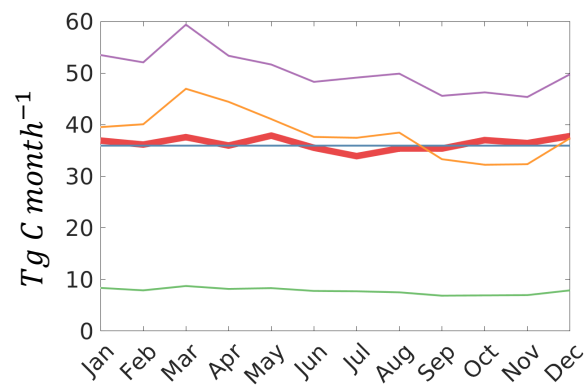

N. STA

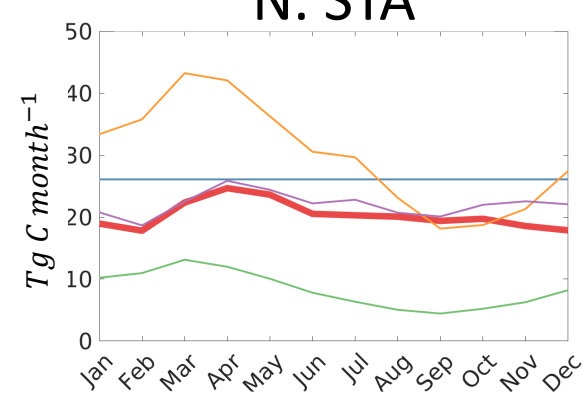

N. Indian

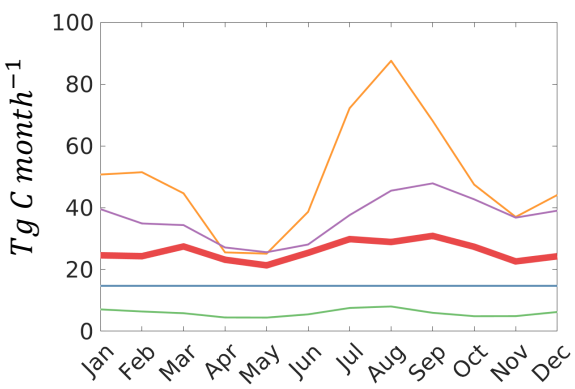

S. Indian

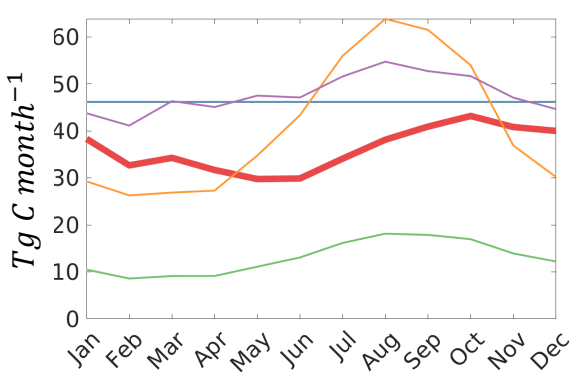

S. TP

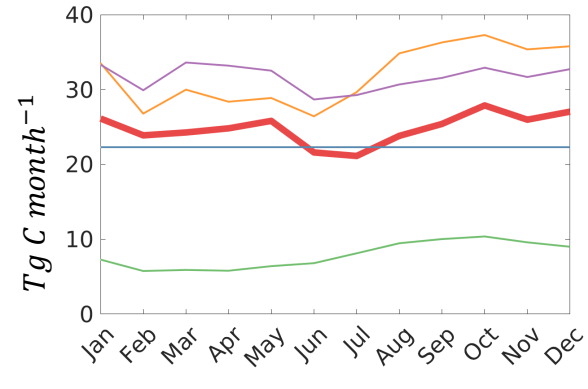

S. TA

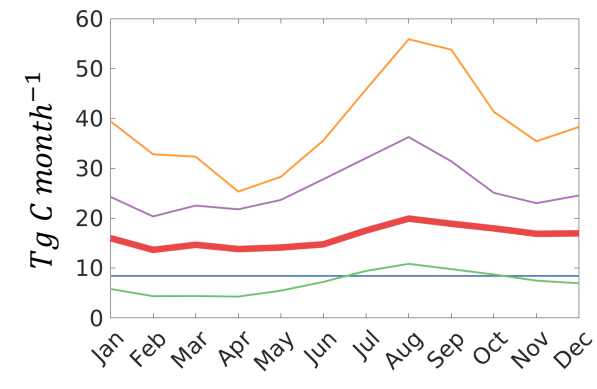

S. STP

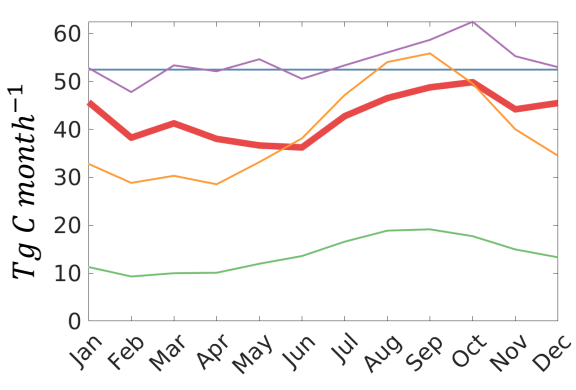

S. STA

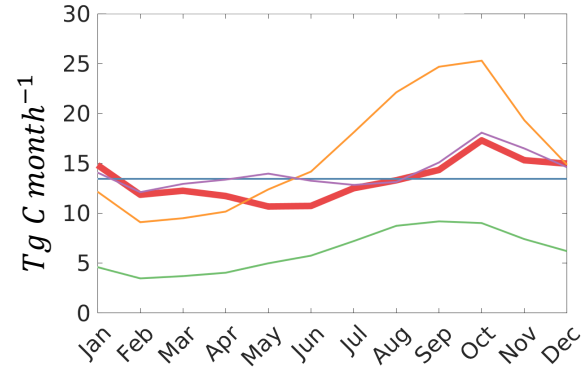

SAZ

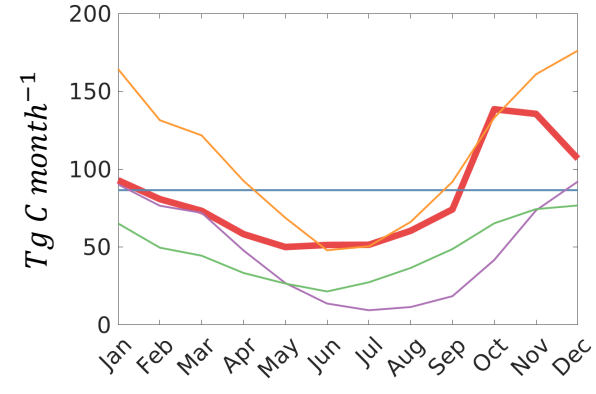

AAZ

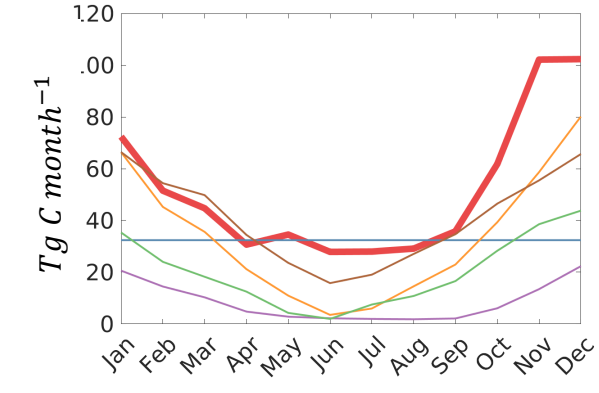

Figure 7.

a) This Study

b). Arteaga - vgpm

c) Arteaga - Marra

d) Arteaga - Carr

e) Arteaga - Cbpm

f) Arteaga - Mean

150
100
50
0

$\frac{\text{mg Carbon}}{\text{m}^2 \cdot \text{day}}$

g)

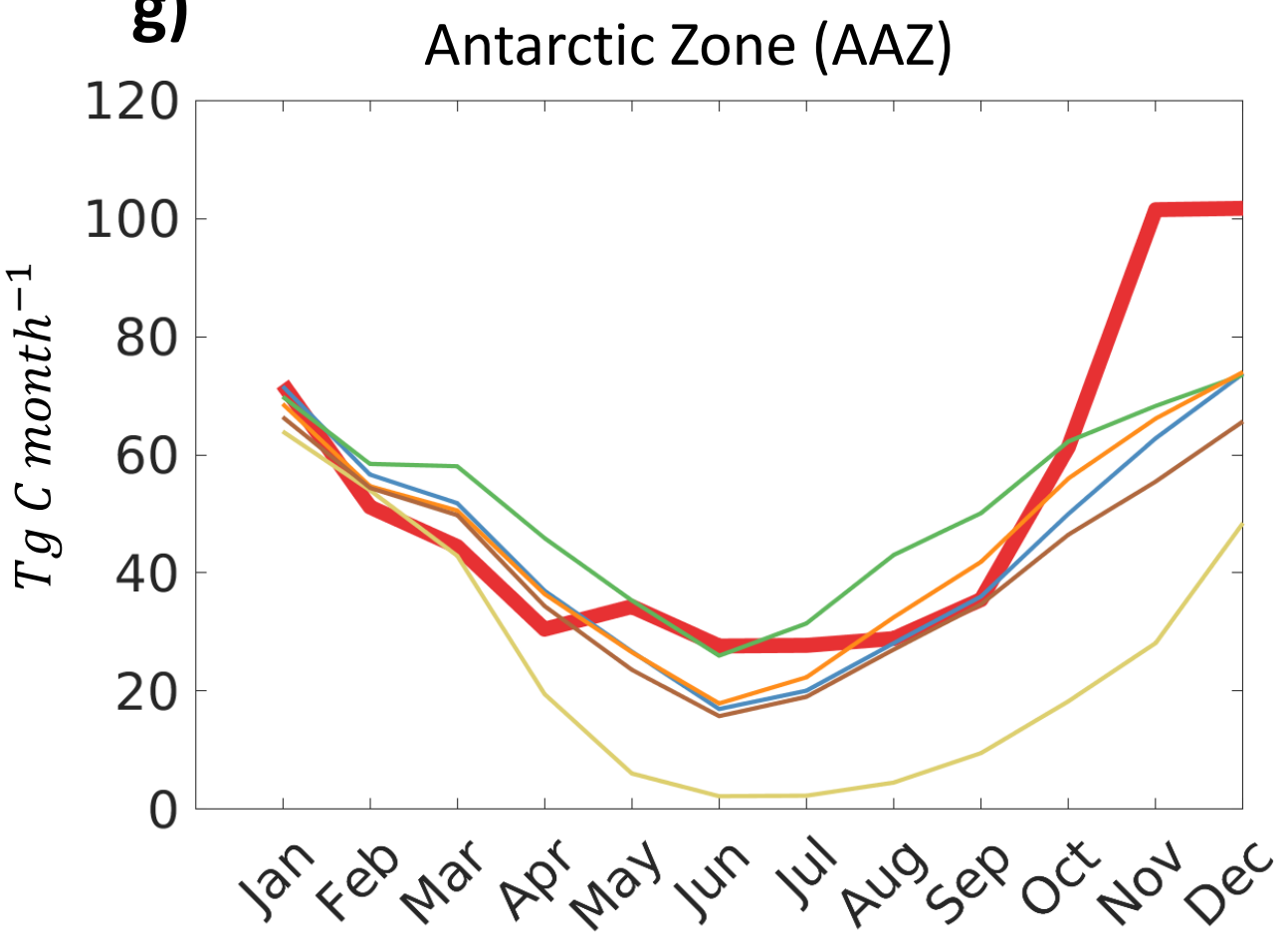

Figure 8.

a)

Annual average POC flux from the wintertime Mixed Layer

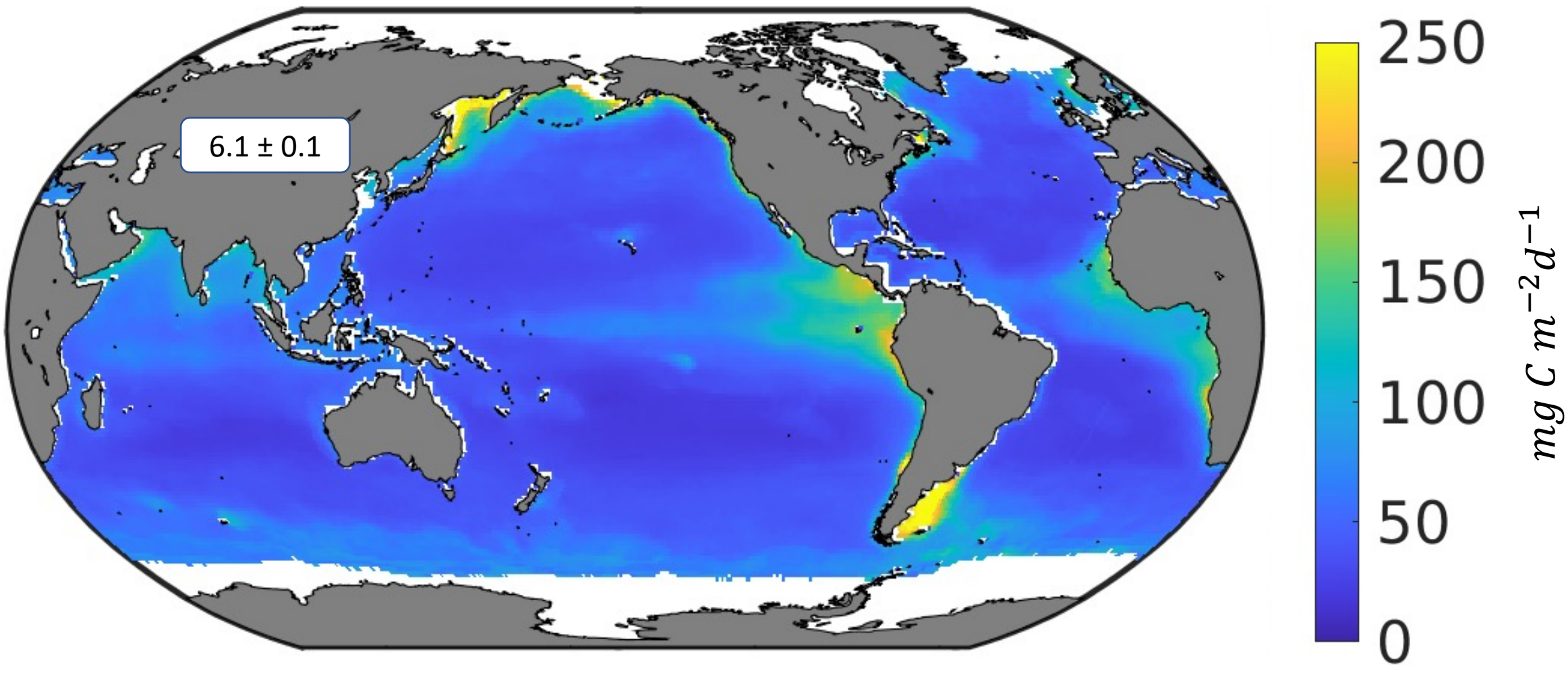

b)

Ratio of Annual average POC flux from maximum Mixed Layer depth to Euphotic depth

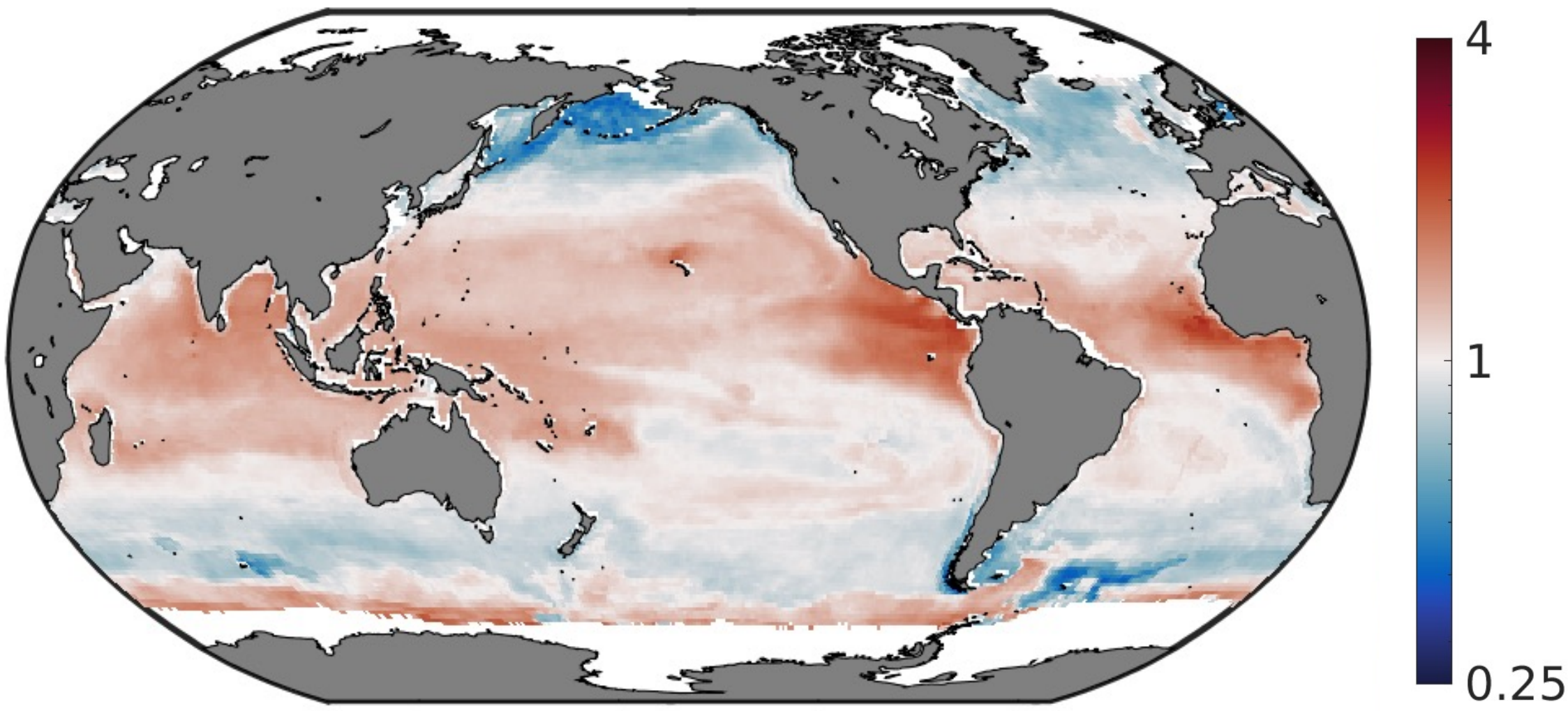

c)

Ratio of Annual average Euphotic depth to maximum Mixed Layer depth